

Thymocytes trigger self-antigen-controlling pathways in immature medullary thymic epithelial stages

Noella Lopes¹, Nicolas Boucherit^{1†}, Jérémy C Santamaria^{1†}, Nathan Provin^{2†}, Jonathan Charaix¹, Pierre Ferrier¹, Matthieu Giraud², Magali Irla^{1*}

¹Aix-Marseille University, CNRS, INSERM, Centre d'Immunologie de Marseille-Luminy, Marseille, France; ²Nantes Université, INSERM, Center for Research in Transplantation and Translational Immunology, UMR 1064, Nantes, France

Abstract Interactions of developing T cells with Aire⁺ medullary thymic epithelial cells expressing high levels of MHCII molecules (mTEC^{hi}) are critical for the induction of central tolerance in the thymus. In turn, thymocytes regulate the cellularity of Aire⁺ mTEC^{hi}. However, it remains unknown whether thymocytes control the precursors of Aire⁺ mTEC^{hi} that are contained in mTEC^{lo} cells or other mTEC^{lo} subsets that have recently been delineated by single-cell transcriptomic analyses. Here, using three distinct transgenic mouse models, in which antigen presentation between mTECs and CD4⁺ thymocytes is perturbed, we show by high-throughput RNA-seq that self-reactive CD4⁺ thymocytes induce key transcriptional regulators in mTEC^{lo} and control the composition of mTEC^{lo} subsets, including Aire⁺ mTEC^{hi} precursors, post-Aire and tuft-like mTECs. Furthermore, these interactions upregulate the expression of tissue-restricted self-antigens, cytokines, chemokines, and adhesion molecules important for T-cell development. This gene activation program induced in mTEC^{lo} is combined with a global increase of the active H3K4me3 histone mark. Finally, we demonstrate that these self-reactive interactions between CD4⁺ thymocytes and mTECs critically prevent multiorgan autoimmunity. Our genome-wide study thus reveals that self-reactive CD4⁺ thymocytes control multiple unsuspected facets from immature stages of mTECs, which determines their heterogeneity.

*For correspondence: Magali.Irla@inserm.fr

†These authors contributed equally to this work

Competing interest: The authors declare that no competing interests exist.

Funding: See page 26

Preprinted: 29 November 2020

Received: 03 May 2021

Accepted: 14 January 2022

Published: 21 February 2022

Reviewing Editor: Sarah Russell, Peter MacCallum Cancer Centre, Australia

© Copyright Lopes et al. This article is distributed under the terms of the [Creative Commons Attribution License](https://creativecommons.org/licenses/by/4.0/), which permits unrestricted use and redistribution provided that the original author and source are credited.

Editor's evaluation

This manuscript is of interest to readers in the field of immunology and especially in the induction of immune tolerance in the thymus. The work uses several mouse models to substantially broaden the current understanding of MHCII/TCR-mediated cell-cell crosstalk in the thymus and suggests a novel mechanism that contributes to the generation of functional and self-tolerant T-cells.

Introduction

The thymic medulla ensures the generation of a self-tolerant T-cell repertoire (Klein et al., 2014; Lopes et al., 2015). By their unique ability to express tissue-restricted self-antigens (TRAs) (Derbinski et al., 2001; Sansom et al., 2014), medullary thymic epithelial cells (mTECs) promote the development of Foxp3⁺ regulatory T cells and the deletion by apoptosis of self-reactive thymocytes capable of inducing autoimmunity (Klein et al., 2019). The expression of TRAs that mirrors body's self-antigens is controlled by Aire (Autoimmune regulator) and Fezf2 (Fez family zinc finger 2) transcription factors (Anderson et al., 2002; Takaba et al., 2015). Aire-dependent TRAs are generally characterized by a repressive chromatin state enriched in the trimethylation of lysine-27 of histone H3 (H3K27me3)

histone mark (*Handel et al., 2018; Org et al., 2009; Sansom et al., 2014*). In accordance with their essential role in regulating the expression of TRAs, *Aire*^{-/-} and *Fezf2*^{-/-} mice show defective clonal deletion of autoreactive thymocytes and develop signs of autoimmunity in several peripheral tissues (*Anderson et al., 2002; Takaba et al., 2015*).

Based on the level of the co-expressed MHC class II and CD80 molecules, mTECs were initially subdivided into mTEC^{lo} (MHCII^{lo}CD80^{lo}) and mTEC^{hi} (MHCII^{hi}CD80^{hi}) (*Gray et al., 2006*). The relationship between these two subsets has been established with reaggregate thymus organ cultures in which mTEC^{lo} give rise to mature Aire⁺ mTEC^{hi} (*Gäbler et al., 2007; Gray et al., 2007*). Although mTEC^{hi} express a highly diverse array of TRAs under Aire's action that releases stalled RNA polymerase and modulates chromatin accessibility, mTEC^{lo} already express a substantial amount of TRAs (*Derbinski et al., 2005; Giraud et al., 2012; Koh et al., 2018; Kyewski and Klein, 2006; Sansom et al., 2014*). Recent single-cell transcriptomic analyses indicate that the heterogeneity of mTECs, especially in the mTEC^{lo} compartment, is more complex than previously thought (*Irla, 2020; Kadouri et al., 2020*). mTEC^{lo} with low or no expression of CD80 have been shown to be divided into three main subsets: CCL21⁺ mTECs, implicated in the attraction of positively selected thymocytes in the medulla (*Lkhagvasuren et al., 2013*), involucrin⁺TPA^{hi} post-Aire mTECs corresponding to the ultimate mTEC differentiation stage (*Metzger et al., 2013; Michel et al., 2017; Nishikawa et al., 2010*), and the newly reported tuft-like mTECs that show properties of gut chemosensory epithelial tuft cells expressing the doublecortin-like kinase 1 (DCLK1) marker (*Bornstein et al., 2018; Miller et al., 2018*). Based on single-cell transcriptomic analyses, mTECs were then classified into four major groups encompassing mTEC I:CCL21⁺ mTECs, mTEC II:Aire⁺ mTECs, mTEC III:post-Aire mTECs, and mTEC IV:tuft-like mTECs (*Bornstein et al., 2018*). Furthermore, mTEC^{lo} with intermediate levels of CD80 and MHCII lie into mTEC single-cell clusters that are defined as proliferating and maturational, expressing *Fezf2* and preceding the Aire⁺ mTEC^{hi} stage (*Baran-Gale et al., 2020; Dhalla et al., 2020*). These transit-amplifying cells were recently referred to as TAC-TECs (*Wells et al., 2020*).

In the postnatal thymus, while mTECs control the selection of thymocytes, conversely CD4⁺ thymocytes control the cellularity of Aire⁺ mTEC^{hi} by activating RANK and CD40-induced NF- κ B signaling pathways (*Akiyama et al., 2008; Hikosaka et al., 2008; Irla, 2020; Irla et al., 2008*). These bidirectional interactions between mTECs and thymocytes are commonly referred to as thymic crosstalk (*Lopes et al., 2015; van Ewijk et al., 1994*). However, it remains unknown whether CD4⁺ thymocytes act exclusively on mature Aire⁺ mTEC^{hi} or upstream on their TAC-TEC precursors contained in mTEC^{lo} and whether the development of the newly identified *Fezf2*⁺, post-Aire, and tuft-like subsets is regulated or not by CD4⁺ thymocytes.

In this study, using high-throughput RNA-sequencing (RNA-seq), we show that self-reactive CD4⁺ thymocytes induce in mTEC^{lo} pivotal transcriptional regulators for their differentiation and function. Accordingly, self-reactive CD4⁺ thymocytes control the composition of the mTEC^{lo} compartment, that is the precursors of Aire⁺ mTEC^{hi}, post-Aire cells, and tuft-like mTECs. Our data also reveal that self-reactive CD4⁺ thymocytes upregulate in mTEC^{lo} the expression of TRAs, chemokines, cytokines, and adhesion molecules involved in T-cell development. This gene activation program correlates with increased levels of the active trimethylation of lysine-4 of histone 3 (H3K4me3) mark, including the loci of *Fezf2*-dependent and Aire/*Fezf2*-independent TRAs, indicative of an epigenetic regulation for their expression. Finally, we demonstrate that disrupted MHCII/TCR interactions between mTECs and CD4⁺ thymocytes lead to the generation of mature T cells containing self-specificities capable of inducing multiorgan autoimmunity. Altogether, our genome-wide study reveals that self-reactive CD4⁺ thymocytes control the developmental transcriptional programs of mTEC^{lo}, which conditions their differentiation and function as inducers of T-cell tolerance.

Results

CD4⁺ thymocytes induce key transcriptional programs in mTEC^{lo} cells

Several NF- κ B members are involved in Aire⁺ mTEC^{hi} development (*Burkly et al., 1995; Lomada et al., 2007; Riemann et al., 2017; Shen et al., 2019; Zhang et al., 2006*). However, it remains unclear whether the NF- κ B or other signaling pathways are activated by CD4⁺ thymocytes specifically in mTEC^{lo} cells. To investigate the effects of CD4⁺ thymocytes in mTEC^{lo}, we used mice deficient in CD4⁺ thymocytes (Δ CD4 mice) because they lack the promoter IV of the class II transactivator

(*Ciita*) gene that controls MHCII expression in cortical TECs (cTECs) (Waldburger et al., 2003). We first analyzed by flow cytometry the total and phosphorylated forms of IKK α , p65, and RelB NF- κ B members and p38 and Erk1/2 MAPK proteins in mTEC^{lo} from Δ CD4 mice according to the gating strategy shown in **Figure 1—figure supplement 1A**. Interestingly, the phosphorylation level of IKK α and p38 MAPK was substantially reduced in Δ CD4 mice (**Figure 1A and B, Figure 1—figure supplement 2**), indicating that CD4⁺ thymocytes may have an impact in mTEC^{lo} by activating the IKK α intermediate of the nonclassical NF- κ B pathway and the p38 MAPK pathway.

To gain insights into the effects of CD4⁺ thymocytes in mTEC^{lo}, we analyzed by high-throughput RNA-seq the gene expression profiles of mTEC^{lo} purified from WT and Δ CD4 mice (**Figure 1—figure supplement 1B**). We found that CD4⁺ thymocytes upregulated 989 genes (fold change [FC] >2) reaching significance for 248 of them (Cuffdiff $p < 0.05$) (**Figure 1C**). 957 genes were also downregulated (FC < 0.5) with 178 genes reaching significance (Cuffdiff $p < 0.05$). We analyzed whether the genes significantly up- or downregulated by CD4⁺ thymocytes corresponded to TRAs, as defined by an expression restricted to 1–5 of peripheral tissues (Sansom et al., 2014). Interestingly, the genes upregulated by CD4⁺ thymocytes exhibited approximately fourfold more of TRAs over non-TRAs (**Figure 1D**, left panel). The comparison of the proportion of TRAs among the upregulated genes with those of the genome revealed a strong statistical TRA overrepresentation ($p = 5.2 \times 10^{-10}$) (**Figure 1D**, right panel). Most of the TRAs upregulated by CD4⁺ thymocytes were sensitive to the action of Aire (Aire-dependent TRAs) or controlled by Aire and Fezf2-independent mechanisms (Aire/Fezf2-independent TRAs) (**Figure 1E, Supplementary file 1**). The upregulation of some of these TRAs by CD4⁺ thymocytes was confirmed by qPCR in mTEC^{lo} purified from Δ CD4 mice (**Figure 1F**). The same results were observed with mTEC^{lo} purified from MHCII^{-/-} mice, also lacking CD4⁺ thymocytes, excluding any potential indirect effect of CIITA in the phenotype observed in Δ CD4 mice (**Figure 1—figure supplement 3A**).

Remarkably, among the non-TRAs upregulated by CD4⁺ thymocytes in mTEC^{lo}, 37 corresponded to 50 mTEC-specific transcription factors that are induced by the histone deacetylase 3 (HDAC3) (Goldfarb et al., 2016; **Figure 1G**). Some of them, such as the interferon regulatory factor 4 (*Irf4*), *Irf7*, and the Ets transcription factor member, *Spib*, are known to regulate mTEC differentiation and function (Akiyama et al., 2014; Haljasorg et al., 2017; Otero et al., 2013). We also identified other transcription factors such as *Nfkb2*, *Trp53*, and *Relb* implicated in mTEC differentiation (Riemann et al., 2017; Rodrigues et al., 2017; Zhang et al., 2006). Finally, we found that CD4⁺ thymocytes upregulate in mTEC^{lo} the expression of some cytokines and cell adhesion molecules such as integrins and cadherins (**Figure 1H, Figure 1—figure supplement 3B**). Given that mTEC^{lo} are heterogeneous (Irla, 2020; Kadouri et al., 2020), we then analyzed whether the cytokines and adhesion molecules, which are upregulated by CD4⁺ thymocytes, are specific to a particular subset of mTEC^{lo}. To this end, we reanalyzed single-cell RNA-seq data performed on total CD45⁺EpCAM⁺ TECs (Wells et al., 2020). Single cells were projected into a UMAP reduced-dimensional space and, using the 15 first principal components, six clusters were obtained, as in Wells et al., 2020 (**Figure 1—figure supplement 4A**). Well-established markers were used to distinguish the different TEC subsets such as *Psemb11* and *Prss16* for cTECs, *Ccl21a* and *Krt5* for CCL21⁺ mTECs (also called mTEC I), *Stmn1*, *Ska1*, *Fezf2* and *Aire* for TAC-TECs, *Aire* and *Fezf2* for Aire⁺ mTECs (also called mTEC II), *Pigr* and *Cldn3* for post-Aire mTECs (also called mTEC III), and *Avil* and *Pou2f3* for tuft-like mTECs (also called mTEC IV) (**Figure 1—figure supplement 4B**). In contrast to CCL21⁺ mTECs, some genes upregulated by CD4⁺ thymocytes were expressed by tuft-like mTECs (**Figure 1I**). Interestingly, many genes encoding for cytokines and cell adhesion molecules were associated with Aire⁺ mTECs and post-Aire cells with some of them already expressed in TAC-TECs, suggesting that CD4⁺ thymocytes may act upstream of Aire⁺ mTEC^{hi}. These results thus provide the first evidence that CD4⁺ thymocytes are able to induce in mTEC^{lo} essential transcriptional regulators for mTEC differentiation and function as well as TRAs, adhesion molecules, and cytokines.

CD4⁺ thymocytes regulate maturational programs in mTEC^{lo} through MHCII/TCR interactions

We next investigated by which mechanism CD4⁺ thymocytes regulate the transcriptional programs of mTEC^{lo}. Given that MHCII/TCR interactions with mTECs are critical for CD4⁺ T-cell selection (Klein et al., 2019), we hypothesized that these interactions could play an important role in initiating

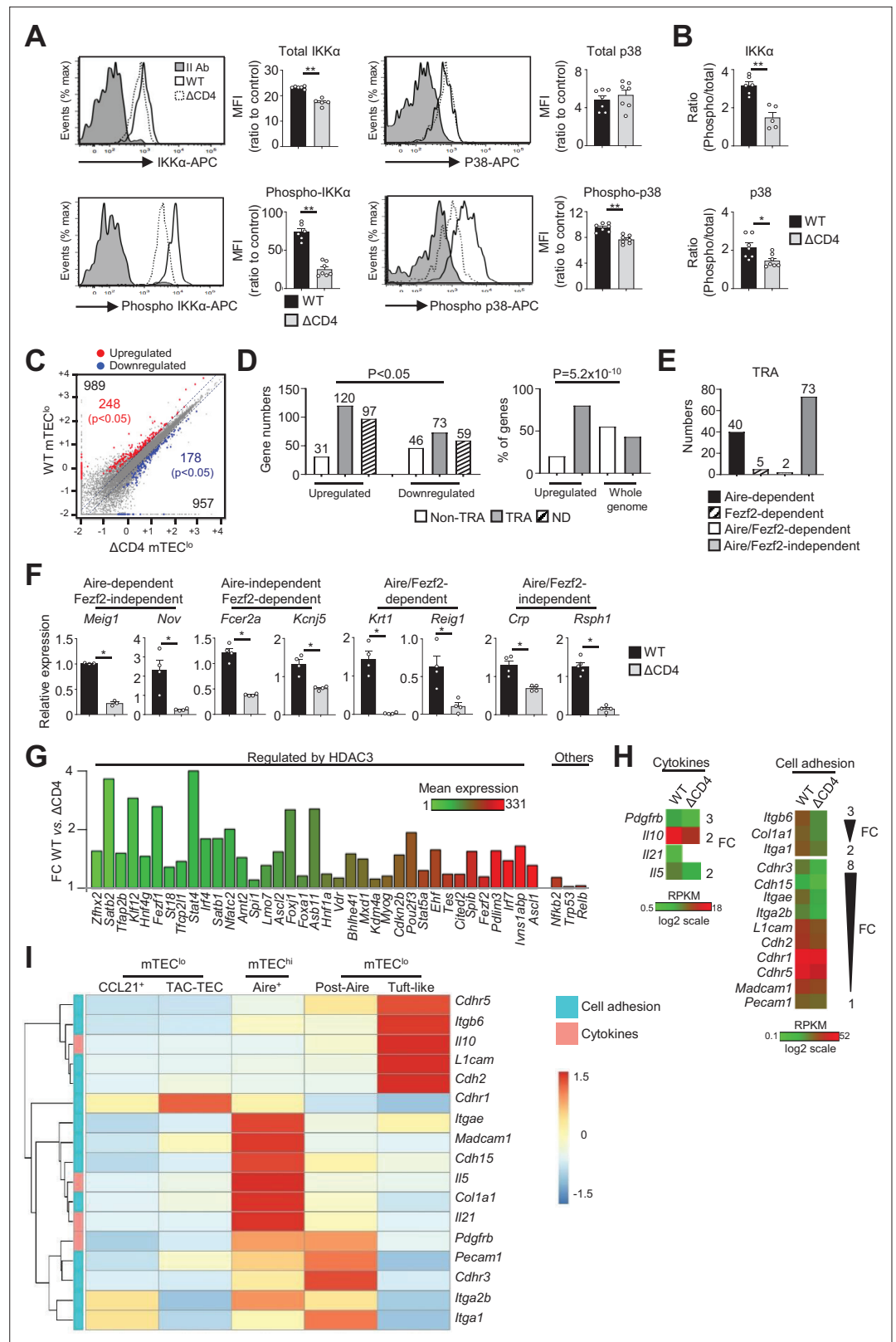


Figure 1. The transcriptional profile and IKKα and p38 MAPK signaling pathways are impaired in mTEC^{lo} of ΔCD4 mice. (A, B) Total IKKα, p38 MAPK, phospho-IKKα(Ser180)/IKKβ(Ser181), and p38 MAPK (Thr180/Tyr182) (A) and the ratio of phospho/total proteins (B) analyzed by flow cytometry in mTEC^{lo} from WT and ΔCD4 mice. Data are representative of two independent experiments (n = 3–4 mice per group and experiment). (C) Scatter

Figure 1 continued on next page

Figure 1 continued

plot of gene expression levels (fragments per kilobase of transcript per million mapped reads [FPKM]) of mTEC^{lo} from WT versus Δ CD4 mice. Genes with fold difference ≥ 2 and $p\text{-adj} < 0.05$ were considered as upregulated or downregulated genes (red and blue dots, respectively). RNA-seq was performed on two independent biological replicates with mTEC^{lo} derived from 3 to 5 mice. (D) Numbers of tissue-restricted self-antigens (TRAs) and non-TRAs in genes up- and downregulated (left panel) and the proportion of upregulated TRAs compared to those in the all genome (right panel). ND, not determined. (E) Numbers of induced Aire-dependent, Fezf2-dependent, Aire/Fezf2-dependent, and Aire/Fezf2-independent TRAs. (F) The expression of Aire-dependent (*Meig1*, *Nov*), Fezf2-dependent (*Fcer2a*, *Kcnj5*), Aire/Fezf2-dependent (*Krt1*, *Reig1*), and Aire/Fezf2-independent (*Crp*, *Rsph1*) TRAs measured by qPCR in WT (n = 3–4) and Δ CD4 (n = 3–4) mTEC^{lo}. (G) Expression fold change in HDAC3-induced transcriptional regulators and other transcription factors significantly upregulated in WT versus Δ CD4 mTEC^{lo}. The color code represents gene expression level. (H) Heatmaps of genes encoding for cell adhesion molecules and cytokines that were significantly downregulated in mTEC^{lo} from Δ CD4 mice. (I) Hierarchical clustering and heatmap of mean expression of these cell adhesion molecules and cytokines in mTEC subsets identified by scRNA-seq. Error bars show mean \pm SEM, * $p < 0.05$, ** $p < 0.01$ using two-tailed Mann–Whitney test for (A), (B) and (F) and chi-squared test for (D).

The online version of this article includes the following figure supplement(s) for figure 1:

Figure supplement 1. Gating strategy used to purify mTEC^{lo} cells.

Figure supplement 2. Normal total and phosphorylated p65, RelB, and Erk1/2 proteins in mTEC^{lo} from Δ CD4 mice.

Figure supplement 3. Impaired TRA expression in mTEC^{lo} from MHCII^{-/-} mice.

Figure supplement 4. Identification of thymic epithelial cell (TEC) subsets by single-cell RNA-seq.

transcriptional programs that govern the functional and developmental properties of mTEC^{lo}. To this end, we used a unique transgenic mouse model in which MHCII expression is selectively abrogated in mTECs (mTEC ^{Δ MHCII} mice) (Irla et al., 2008). In contrast to their WT counterparts, we found that OVA₃₂₃₋₃₃₉-loaded mTECs from mTEC ^{Δ MHCII} mice were ineffective at activating OTII-specific CD4⁺ T cells, demonstrating that the capacity of antigen presentation of mTECs to CD4⁺ T cells is impaired in these mice (Figure 2A).

The comparison of the gene expression profiles of mTEC^{lo} purified from WT and mTEC ^{Δ MHCII} mice (Figure 1—figure supplement 1B) revealed that MHCII/TCR interactions with CD4⁺ thymocytes resulted in the upregulation of 1300 genes (FC > 2), 449 of them reaching statistical significance (Cuffdiff $p < 0.05$). 846 genes were also downregulated (FC < 0.5) with 340 reaching significance (Cuffdiff $p < 0.05$) (Figure 2B). Similarly to the comparison of WT versus Δ CD4 mice (Figure 1D), the genes significantly upregulated by MHCII/TCR interactions in mTEC^{lo} corresponded preferentially to TRAs ($p = 4.5 \times 10^{-13}$) that are mainly Aire-dependent and Aire/Fezf2-independent (Figure 2C–E, Supplementary file 2). In line with the recent discovery of Aire expression in mTECs expressing intermediate levels of CD80 identified in the proliferating and maturational stage mTEC single-cell clusters (Dhalla et al., 2020), we found a strong correlation ($p = 2 \times 10^{-16}$) between gene upregulation induced by MHCII/TCR interactions and the responsiveness of genes to Aire's action obtained from the comparison between WT and Aire^{-/-} mTEC^{hi} (Figure 2F). These data are in agreement with the identification of a list of activation factors including Aire among the non-TRA genes induced by MHCII/TCR interactions with CD4⁺ thymocytes in mTEC^{lo} (Figure 2G). mTEC^{lo} from mTEC ^{Δ MHCII} mice expressed ~4.5-fold less Aire than WT mTEC^{lo}, with substantial levels of 15.8 and 73.7 fragments per kilobase of transcript per million mapped reads (FPKM), respectively. For comparison, Aire expression level in WT mTEC^{hi} was 448.9 FPKM. mTEC^{lo} from mTEC ^{Δ MHCII} mice also expressed ~1.5-fold less Fezf2 than WT mTEC^{lo} (90.2 versus 134.5 FPKM, respectively). This reduction in Aire and Fezf2 expression in mTEC ^{Δ MHCII} mice was also confirmed by qPCR (Figure 2H). These results highlight the importance of MHCII/TCR interactions with CD4⁺ thymocytes in upregulating Aire and Fezf2 mRNAs and some of their associated TRAs in mTEC^{lo}. Interestingly, 17 HDAC3-regulated transcription factors as well as *Nfkb2*, *Trp53*, and *Relb* transcription factors were induced by MHCII/TCR interactions with CD4⁺ thymocytes (Figure 2I). Moreover, the expression of several cytokines, chemokines, and cell adhesion molecules was also upregulated (Figure 2J, Figure 2—figure supplement 1A). Using single-cell RNA-seq data (Figure 1—figure supplement 4), we found that these genes were poorly associated with CCL21⁺ and tuft-like mTEC^{lo} (Figure 2K). Consistently with the altered cellularity of Aire⁺ mTECs in mTEC ^{Δ MHCII}

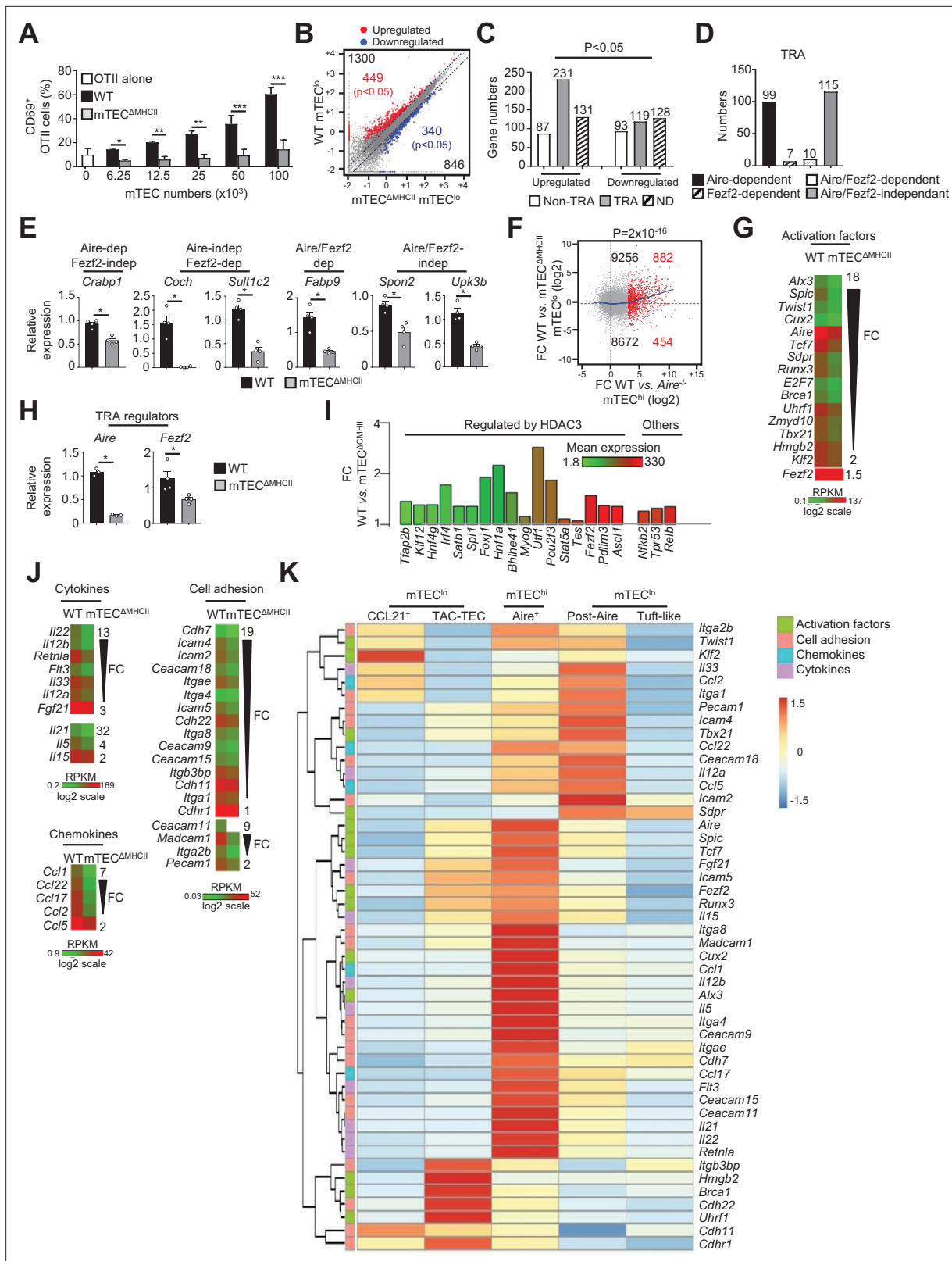


Figure 2. The transcriptional and functional properties of mTEC^{lo} are impaired in mTEC^{ΔMHCII} mice. **(A)** Percentages of CD69⁺ OTII CD4⁺ T cells cultured or not with variable numbers of OVA₃₂₃₋₃₃₉-loaded WT or mTEC^{ΔMHCII} mTECs derived from two independent experiments (n = 2–3 mice per group and experiment). **(B)** Scatter plot of gene expression levels (fragments per kilobase of transcript per million mapped reads [FPKM]) of mTEC^{lo} from WT versus mTEC^{ΔMHCII} mice. Genes with fold difference ≥2 and p-adj < 0.05 were considered as upregulated or downregulated genes (red and blue dots,

Figure 2 continued on next page

Figure 2 continued

respectively). RNA-seq was performed on two independent biological replicates with mTEC^{lo} derived from 3 to 5 mice. (C) Numbers of tissue-restricted self-antigens (TRAs) and non-TRAs in genes up- and downregulated in mTEC^{lo} from WT versus mTEC^{ΔMHCII} mice. ND, not determined. (D) Numbers of induced TRAs regulated or not by Aire and/or Fezf2. (E) Aire-dependent (*Crabp1*), Fezf2-dependent (*Coch*, *Sult1c2*), Aire/Fezf2-dependent (*Fabp9*), and Aire/Fezf2-independent (*Spon2*, *Upk3b*) TRAs were measured by qPCR in mTEC^{lo} from WT (n = 4) and mTEC^{ΔMHCII} (n = 4) mice. (F) Scatter plot of gene expression variation in mTEC^{lo} from WT versus mTEC^{ΔMHCII} mice and in mTEC^{hi} from WT versus *Aire*^{-/-} mice. The loess fitted curve is shown in blue and the induced Aire-dependent genes (fold change [FC] > 5) in red. (G) Heatmap of significantly downregulated activation factors in mTEC^{lo} from mTEC^{ΔMHCII} mice. (H) *Aire* and *Fezf2* mRNAs were measured by qPCR in mTEC^{lo} from WT (n = 3–4) and mTEC^{ΔMHCII} (n = 4) mice. (I) FC in the expression of HDAC3-induced transcriptional regulators and other transcription factors significantly upregulated in WT versus mTEC^{ΔMHCII} mice. The color code represents gene expression level. (J) Heatmap of significantly downregulated cytokines, chemokines, and cell adhesion molecules in mTEC^{lo} from mTEC^{ΔMHCII} mice. (K) Hierarchical clustering and heatmap of mean expression of these activation factors, cell adhesion molecules, chemokines, and cytokines in mTEC subsets identified by scRNA-seq. Error bars show mean ± SEM, *p<0.05, **p<0.01, ***p<0.001 using two-tailed Mann–Whitney test for (A), (E) and (H) and chi-squared test for (C) and (F).

The online version of this article includes the following figure supplement(s) for figure 2:

Figure supplement 1. Altered expression of some cytokines, cell adhesion molecules, and chemokines in mTEC^{lo} from mTEC^{ΔMHCII} mice.

mice (Irla et al., 2008), some of these genes were associated with post-Aire cells. Strikingly, many genes upregulated by CD4⁺ thymocytes in mTEC^{lo} were highly expressed by Aire⁺ mTECs. Interestingly, several of these genes were already expressed by TAC-TECs, including *Aire* and *Fezf2*, strongly suggesting that an enhanced transcriptional activity promoted by MHCII/TCR interactions with CD4⁺ thymocytes accompanies the transition from TAC-TECs to Aire⁺ mTECs. Altogether, these data show that CD4⁺ thymocytes, through MHCII/TCR interactions, control the functional properties of mTEC^{lo} and activate key transcriptional programs governing their differentiation and function.

TCR/MHCII interactions with CD4⁺ thymocytes regulate the development of Fezf2⁺ pre-Aire, post-Aire, and tuft-like mTEC subsets

Since key transcription factors implicated in mTEC differentiation were upregulated in mTEC^{lo} by MHCII/TCR-mediated interactions with CD4⁺ thymocytes (Figures 1G and 2I), we next analyzed the composition for the newly identified mTEC subsets in ΔCD4 and mTEC^{ΔMHCII} mice. In agreement with our previous study (Irla et al., 2008), we first observed a substantial reduction in the frequencies and numbers of mTEC^{hi} in both mice (Figure 3A). Furthermore, numbers of mTEC^{lo} were also substantially reduced. Consequently, ΔCD4 and mTEC^{ΔMHCII} mice have a globally reduced cellularity in total mTECs. An Aire/Fezf2 co-staining both by histology and flow cytometry then revealed a substantial reduction in Aire⁻Fezf2⁺ and Aire⁺Fezf2⁺ cells (Figure 3B and C). We further analyzed by flow cytometry Aire and Fezf2 expression specifically in mTEC^{lo} and mTEC^{hi}, according to the gating strategy shown in Figure 1—figure supplement 1A. In agreement with the detection of Aire in the proliferating and maturational single-cell clusters in mTEC^{lo} (Baran-Gale et al., 2020; Dhalla et al., 2020; Wells et al., 2020), we found that Aire protein was expressed in a small fraction of mTEC^{lo} compared to mTEC^{hi} in WT, ΔCD4, and mTEC^{ΔMHCII} mice (Figure 3C). Aire⁻Fezf2⁺ and Aire⁺Fezf2⁺ mTECs were reduced in mTEC^{lo} of ΔCD4 and mTEC^{ΔMHCII} mice with a more marked effect in mTEC^{hi}. This decrease was not due to impaired proliferation since normal frequencies of Ki-67⁺ proliferating cells were observed in ΔCD4 and mTEC^{ΔMHCII} mice (Figure 3—figure supplement 1). Furthermore, numbers of involucrin⁺TPA⁺Aire⁻ post-Aire cells were reduced in the medulla of ΔCD4 and mTEC^{ΔMHCII} mice (Figure 3—figure supplement 2A), consistently with the decrease of Aire⁺ mTEC^{hi} (Figure 3B and C). In contrast, the frequencies of CCL21⁺ cells among mTEC^{lo} were not altered in ΔCD4 and mTEC^{ΔMHCII} mice (Figure 3D). This is in line with the observation that few genes upregulated by TCR/MHCII interactions with CD4⁺ thymocytes were associated with CCL21⁺ mTECs (Figures 1I and 2K). We also analyzed tuft-like mTECs since the expression of the transcription factor *Pou2f3*, known to control the development of this cell type (Bornstein et al., 2018; Miller et al., 2018), was decreased in mTEC^{lo} of ΔCD4 and mTEC^{ΔMHCII} mice (Figures 1G and 2I). We found that numbers of tuft-like mTECs identified by flow cytometry using the DCLK1 marker were reduced in both mice (Figure 3E, Figure 3—figure supplement 2B), indicating that their development is promoted by MHCII/TCR interactions with CD4⁺ thymocytes. Importantly, Aire⁻Fezf2⁺ and Aire⁺Fezf2⁺ mTEC^{lo} and mTEC^{hi} as well as CCL21⁺ and DCLK1⁺ tuft-like mTEC^{lo} were similarly reduced in MHCII^{-/-} mice, further confirming that CD4⁺ thymocytes control the cellularity of these novel mTEC subsets (Figure 3—figure supplement 3).

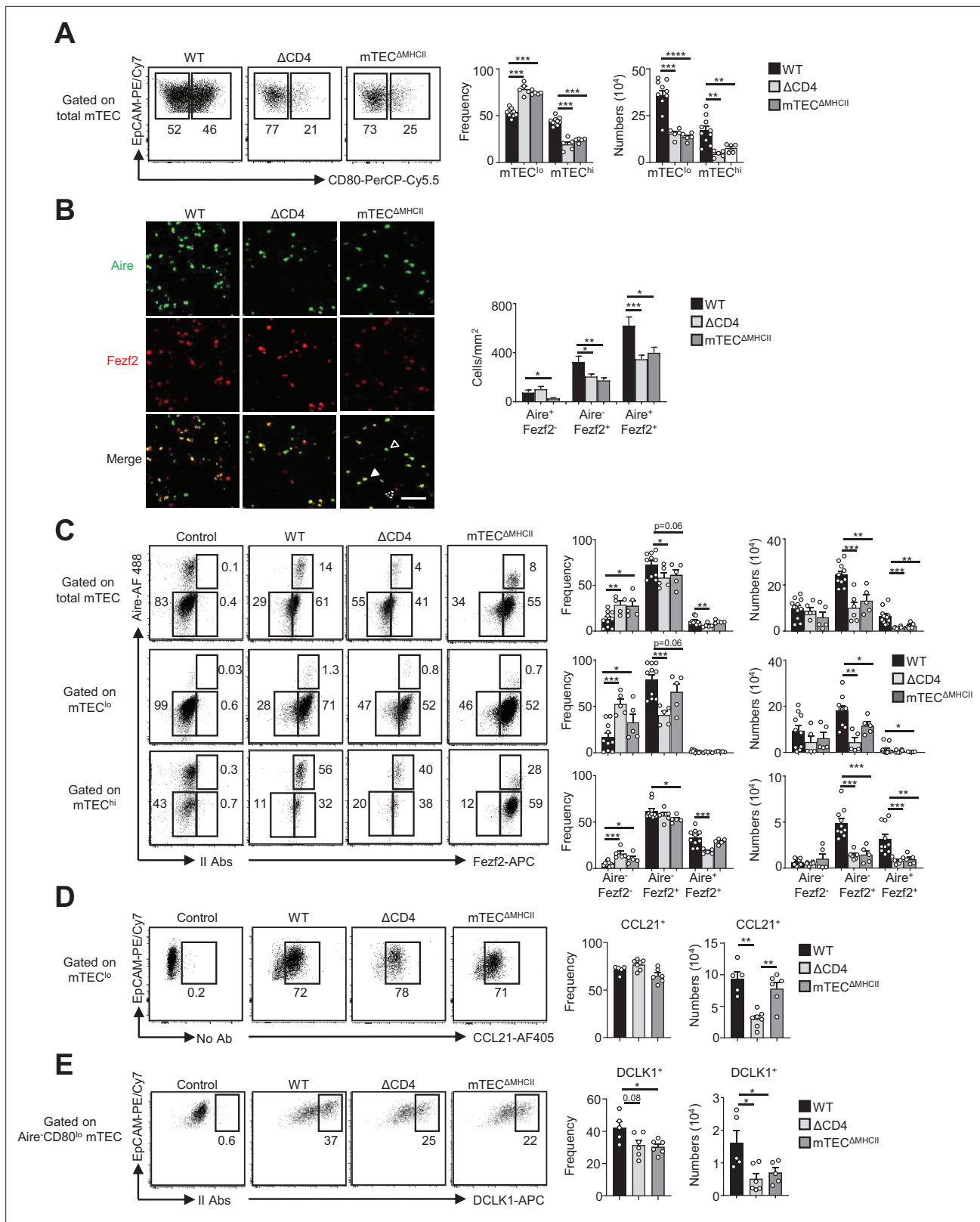


Figure 3. The composition in medullary thymic epithelial cell (mTEC) subsets is altered in Δ CD4 and mTEC ^{Δ MHCI} mice. **(A)** Flow cytometry profiles, frequencies, and numbers of mTEC^{lo} and mTEC^{hi} in WT, Δ CD4, and mTEC ^{Δ MHCI} mice. Data are representative of 2–3 independent experiments (n = 2–5 mice per group and experiment). **(B)** Confocal images of thymic sections from WT, Δ CD4, and mTEC ^{Δ MHCI} mice stained for Aire (green) and Fezf2 (red). 12 and 20 sections derived from two WT, two Δ CD4, and two mTEC ^{Δ MHCI} mice were quantified. Scale bar, 50 μ m. Unfilled, dashed and

Figure 3 continued on next page

Figure 3 continued

solid arrowheads indicate Aire⁺Fezf2⁻, Aire⁻Fezf2⁺, and Aire⁺Fezf2⁺ cells, respectively. The histogram shows the density of Aire⁺Fezf2⁻, Aire⁻Fezf2⁺, and Aire⁺Fezf2⁺ cells. (C–E) Flow cytometry profiles, frequencies, and numbers of Aire⁻Fezf2⁻, Aire⁻Fezf2⁺, and Aire⁺Fezf2⁺ cells in total mTECs, mTEC^{lo}, and mTEC^{hi} (C), of CCL21⁺ cells in mTEC^{lo} (D) and of DCKL1⁺ cells in Aire⁻ mTEC^{lo} (E) from WT, Δ CD4, and mTEC ^{Δ MHCII} mice. II Abs: secondary antibodies. Data are representative of 2–3 independent experiments (n = 2–5 mice per group and experiment). Error bars show mean \pm SEM, *p<0.05, **p<0.01, ***p<0.001, ****p<0.0001 using unpaired Student's t-test for (B) and two-tailed Mann–Whitney test for (A) and (C–E).

The online version of this article includes the following figure supplement(s) for figure 3:

Figure supplement 1. Normal proliferation of Aire⁻Fezf2⁺ and Aire⁺Fezf2⁺ medullary thymic epithelial cell (mTECs) in Δ CD4 and mTEC ^{Δ MHCII} mice.

Figure supplement 2. Reduced post-Aire medullary thymic epithelial cells (mTECs) in Δ CD4 and mTEC ^{Δ MHCII} mice.

Figure supplement 3. Analysis of medullary thymic epithelial cell (mTEC) subsets in MHCII^{-/-} mice.

Altogether, these data reveal that MHCII/TCR-mediated interactions with CD4⁺ thymocytes have a broad impact on mTEC composition by controlling the cellularity of not only Aire⁺Fezf2⁺ mTECs but also Fezf2⁺ pre-Aire⁺ mTECs, post-Aire, and tuft-like cells.

Highly self-reactive CD4⁺ thymocytes activate maturational programs in mTEC^{lo}

We next assessed the impact of highly self-reactive interactions with CD4⁺ thymocytes in mTEC^{lo} using OTII-Rag2^{-/-} and RipmOVAxOTII-Rag2^{-/-} transgenic mice. Both models possess CD4⁺ thymocytes expressing an MHCII-restricted TCR specific for the chicken ovalbumin (OVA). The Rip-mOVA line expresses a membrane-bound OVA form specifically in mTECs, and consequently high-affinity interactions between OVA-expressing mTECs and OTII CD4⁺ thymocytes are only possible in RipmOVAx-OTII-Rag2^{-/-} mice (Kurts et al., 1996). In contrast to total Erk1/2 MAPK, p38 MAPK, IKK α , and p65, the nonclassical NF- κ B subunit RelB was increased in mTEC^{lo} at mRNA and protein levels in RipmOVAx-OTII-Rag2^{-/-} compared to OTII-Rag2^{-/-} mice (Figure 4A and B, Figure 4—figure supplement 1). By reanalyzing single-cell RNA-seq data on mTEC^{lo} subsets, we found that in contrast to CCL21⁺ and tuft-like mTECs Relb is highly expressed by TAC-TECs and post-Aire cells, arguing again in favor that self-reactive CD4⁺ thymocytes act from the TAC-TEC stage to induce their differentiation into Aire⁺ cells and then into post-Aire cells (Figure 4—figure supplement 2A). The level of RelB phosphorylation was also higher in RipmOVAxOTII-Rag2^{-/-} than OTII-Rag2^{-/-} mice (Figure 4B), suggesting that self-reactive CD4⁺ thymocytes may activate the nonclassical NF- κ B pathway in mTEC^{lo}.

To define the genome-wide effects of highly self-reactive CD4⁺ thymocytes in mTEC^{lo}, we compared the gene expression profiles of mTEC^{lo} from RipmOVAxOTII-Rag2^{-/-} versus OTII-Rag2^{-/-} mice (Figure 1—figure supplement 1B) and found an upregulation of 1438 genes (FC > 2) reaching statistical significance for 522 of them (Cuffdiff p<0.05). 620 genes were also downregulated (FC < 0.5) with 136 reaching significance (Cuffdiff p<0.05) (Figure 4C). The genes upregulated exhibited an approximately fourfold more of TRA over non-TRA genes (p=4.7 \times 10⁻²³), which corresponded mainly to Aire-dependent and Aire/Fezf2-independent TRAs (Figure 4D–F, Supplementary file 3). Similarly to the WT versus mTEC ^{Δ MHCII} comparison, we found a strong correlation (p=6.2 \times 10⁻⁷) between the genes upregulated by self-reactive CD4⁺ thymocytes and the responsiveness of genes to Aire's action obtained from the comparison between WT and Aire^{-/-} mTEC^{hi} (Figure 4G). These results support an impact of antigen-specific interactions in the expression of TRAs in mTEC^{lo}, notably on Aire-dependent TRAs. Importantly, these results are in agreement with the induction of a list of activation factors including Aire and Fezf2 among the non-TRA genes (Figure 4H). Similarly to the comparisons of the WT versus Δ CD4 or mTEC ^{Δ MHCII} mice, numerous HDAC3-induced regulators as well as Sirt1, Nfkb2, Relb, and Trp53 transcription factors were upregulated in mTEC^{lo} of RipmOVAx-OTII-Rag2^{-/-} mice compared to OTII-Rag2^{-/-} mice (Figure 4I). Interestingly, 21 out of 30 top targets of the Foxn1 transcription factor, implicated in TEC differentiation and growth (Žuklys et al., 2016), as well as cytokines, chemokines, and cell adhesion molecules, were also upregulated (Figure 4J, K Figure 4—figure supplement 2B). We found that few of these genes were associated with CCL21⁺ and tuft-like mTECs (Figure 4L). In contrast, many genes encoding for activation factors, cytokines, chemokines, and cell adhesion molecules were associated with Aire⁺ and post-Aire mTECs, consistently with the fact that antigen-specific interactions with CD4⁺ thymocytes control the cellularity of Aire⁺ mTECs. Moreover, most of these genes, including Aire and Fezf2, were already expressed by

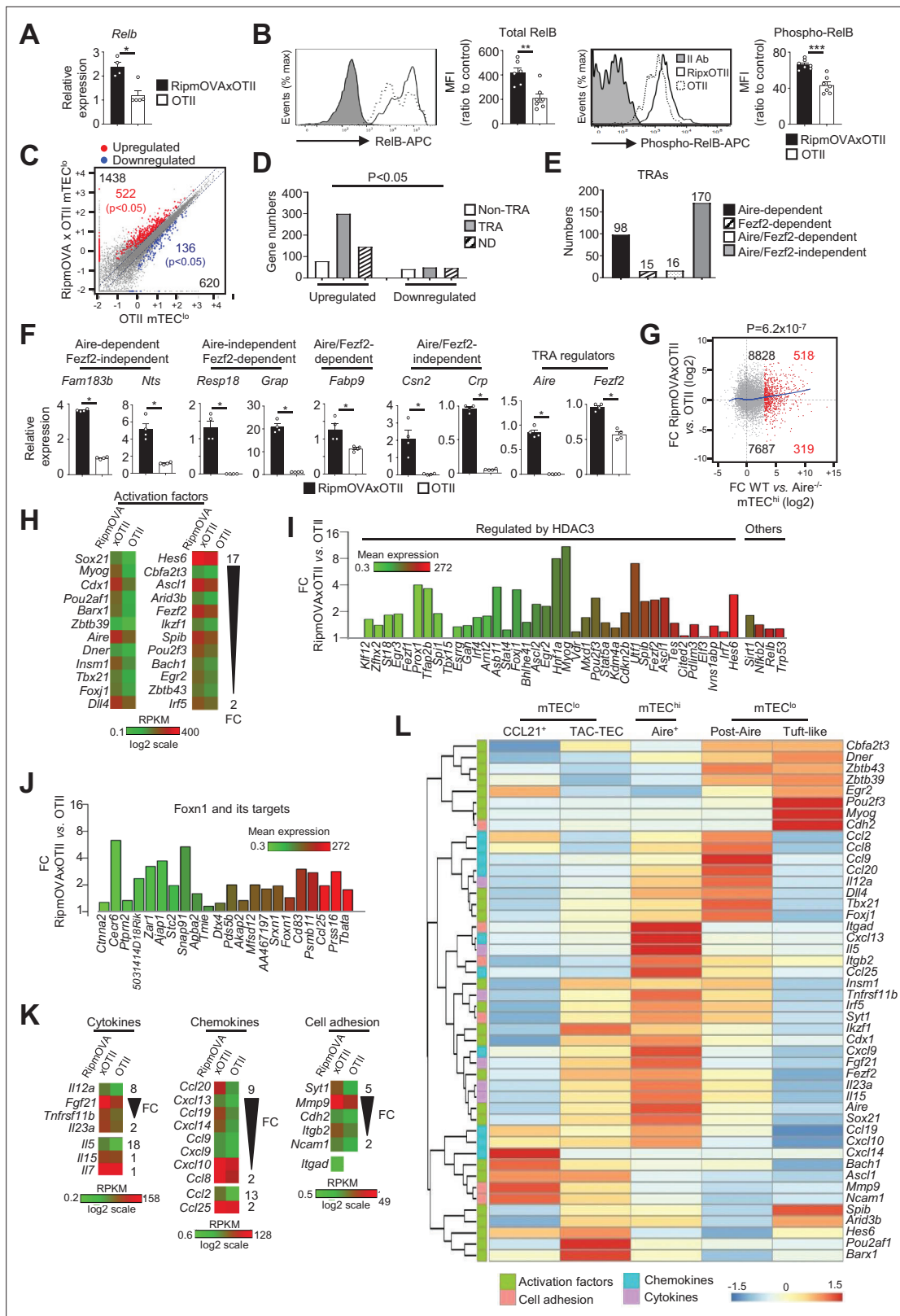


Figure 4. Highly self-reactive CD4⁺ thymocytes control the transcriptional and functional properties of *mTEC^{lo}*. **(A)** *Relb* mRNA was measured by qPCR in *mTEC^{lo}* from *RipmOVAxOTII-Rag2^{-/-}* (n = 4) and *OTII-Rag2^{-/-}* (n = 5) mice. **(B)** Total and phospho-RelB (Ser552) were analyzed by flow cytometry in *mTEC^{lo}* from *RipmOVAxOTII-Rag2^{-/-}* and *OTII-Rag2^{-/-}* mice. Data are representative of two independent experiments (n = 3–4 mice per group and experiment). **(C)** Scatter plot of gene expression levels (fragments per kilobase of transcript per million mapped reads [FPKM]) in *mTEC^{lo}* from

Figure 4 continued on next page

Figure 4 continued

RipmOVAxOTII-Rag2^{-/-} versus OTII-Rag2^{-/-} mice. Genes with fold difference ≥ 2 and $p\text{-adj} < 0.05$ were considered as upregulated or downregulated genes (red and blue dots, respectively). RNA-seq was performed on two independent biological replicates with mTEC^{lo} derived from 5 to 8 mice. (D) Numbers of tissue-restricted self-antigens (TRAs) and non-TRAs in genes up- and downregulated in mTEC^{lo} from RipmOVAxOTII-Rag2^{-/-} versus OTII-Rag2^{-/-} mice. ND, not determined. (E) Numbers of induced Aire-dependent, Fezf2-dependent, Aire/Fezf2-dependent, and Aire/Fezf2-independent TRAs. (F) Aire-dependent (*Fam183b*, *Nts*), Fezf2-dependent (*Resp18*, *Grap*), Aire/Fezf2-dependent (*Fabp9*), Aire/Fezf2-independent (*Csn2*, *Crp*) TRAs, Aire and Fezf2 mRNAs were measured by qPCR in mTEC^{lo} from RipmOVAxOTII-Rag2^{-/-} (n = 4) and OTII-Rag2^{-/-} (n = 4) mice. (G) Scatter plot of gene expression variation in mTEC^{lo} from RipmOVAxOTII-Rag2^{-/-} versus OTII-Rag2^{-/-} mice and in mTEC^{hi} from WT versus Aire^{-/-} mice. The loess fitted curve is shown in blue and induced Aire-dependent genes (fold change [FC] > 5) in red. (H) Heatmap of significantly upregulated activation factors in mTEC^{lo} from RipmOVAxOTII-Rag2^{-/-} compared to OTII-Rag2^{-/-} mice. (I, J) Expression FC in HDAC3-induced transcriptional regulators and other transcription factors (I) and in Foxn1 targets (J) in mTEC^{lo} from RipmOVAxOTII-Rag2^{-/-} versus OTII-Rag2^{-/-} mice. The color code represents gene expression level. (K) Heatmap of significantly upregulated cytokines, chemokines, and cell adhesion molecules in mTEC^{lo} from RipmOVAxOTII-Rag2^{-/-} mice. (L) Hierarchical clustering and heatmap of mean expression of these activation factors, cell adhesion molecules, chemokines, and cytokines in mTEC subsets identified by scRNA-seq. Error bars show mean \pm SEM, * $p < 0.05$, ** $p < 0.01$, *** $p < 0.001$ using two-tailed Mann–Whitney test for (A), (B) and (F) and chi-squared test for (D) and (G).

The online version of this article includes the following figure supplement(s) for figure 4:

Figure supplement 1. Similar levels of total and phosphorylated p65, Erk1/2, p38, and IKK α proteins in mTEC^{lo} from RipmOVAxOTII-Rag2^{-/-} and OTII-Rag2^{-/-} mice.

Figure supplement 2. Expression of *Relb*, cytokines, chemokines, and cell adhesion molecules that was altered in mTEC^{lo} from RipmOVAxOTII-Rag2^{-/-} and OTII-Rag2^{-/-} mice.

TAC-TECs, further highlighting that CD4⁺ thymocytes act upstream of Aire⁺ mTEC^{hi}. Altogether, these data reveal that highly self-reactive CD4⁺ thymocytes control in mTEC^{lo} not only key transcription factors driven by their differentiation but also key molecules for T-cell development and selection such as TRAs, cytokines, chemokines, and adhesion molecules.

Highly self-reactive CD4⁺ thymocytes control mTEC subset composition from a progenitor stage

Given that highly self-reactive CD4⁺ thymocytes induce key transcription factors in mTEC^{lo} (Figure 4H and I), we examined their respective impact on mTEC subset development. Strikingly, numbers of total TECs and mTECs were higher in RipmOVAxOTII-Rag2^{-/-} than in OTII-Rag2^{-/-} mice (Figure 5A and B). We analyzed four TEC subsets based on MHCII and UEA-1 levels, as previously described (Lopes et al., 2017; Wong et al., 2014; Figure 5C). In contrast to cTEC^{hi} (MHCII^{hi}UEA-1^{lo}), numbers of TEC^{lo} (MHCII^{lo}UEA-1^{lo}), mTEC^{lo} (MHCII^{lo}UEA-1⁺), and mTEC^{hi} (MHCII^{hi}UEA-1⁺) were higher in RipmOVAxOTII-Rag2^{-/-} than in OTII-Rag2^{-/-} mice. Consistently, numbers of mTEC^{lo} and mTEC^{hi} identified based on the level of CD80 expression were also higher in RipmOVAxOTII-Rag2^{-/-} mice (Figure 5—figure supplement 1). Interestingly, numbers of $\alpha 6$ -integrin^{hi}Sca-1^{hi} thymic epithelial progenitor (TEPC)-enriched cells in the TEC^{lo} subset were also increased (Figure 5D), indicating that self-reactive CD4⁺ thymocytes control TEC development from a progenitor stage. Of note, this strategy of TEC identification was not possible in Δ CD4 and mTEC ^{Δ MHCII} mice since MHCII expression is abrogated in TECs of these mice (Irla et al., 2008).

A higher density of Aire⁺Fezf2⁻, Aire⁻Fezf2⁺, and Aire⁺Fezf2⁺ cells was observed in medullary regions of RipmOVAxOTII-Rag2^{-/-} mice by immunohistochemistry (Figure 5E). Furthermore, numbers of Aire⁻Fezf2⁻ mTEC^{lo} analyzed by flow cytometry were also higher in RipmOVAxOTII-Rag2^{-/-} mice, confirming that self-reactive CD4⁺ thymocytes control mTEC differentiation from an early stage (Figure 5F). Numbers of Aire⁺Fezf2⁺ and Aire⁻Fezf2⁺ mTEC^{lo} and mTEC^{hi} were also markedly increased in these mice, although similar frequencies of proliferating Ki-67⁺ cells were observed (Figure 5—figure supplement 2). In agreement with increased Aire⁺ mTECs, involucrin⁺T-PA⁺Aire⁻ post-Aire cells were enhanced (Figure 5—figure supplement 3). Furthermore, numbers of CCL21⁺ and DCLK1⁺ tuft-like cells in mTEC^{lo} were also increased in RipmOVAxOTII-Rag2^{-/-} mice compared to OTII-Rag2^{-/-} mice (Figure 5G and H). These observations are consistent with our previous findings that antigen-specific interactions between mTECs and CD4⁺ thymocytes induce medulla development (Irla et al., 2012). Altogether, these results demonstrate that highly self-reactive CD4⁺ thymocytes regulate mTECs from an early to a late developmental stage and thus mTEC composition.

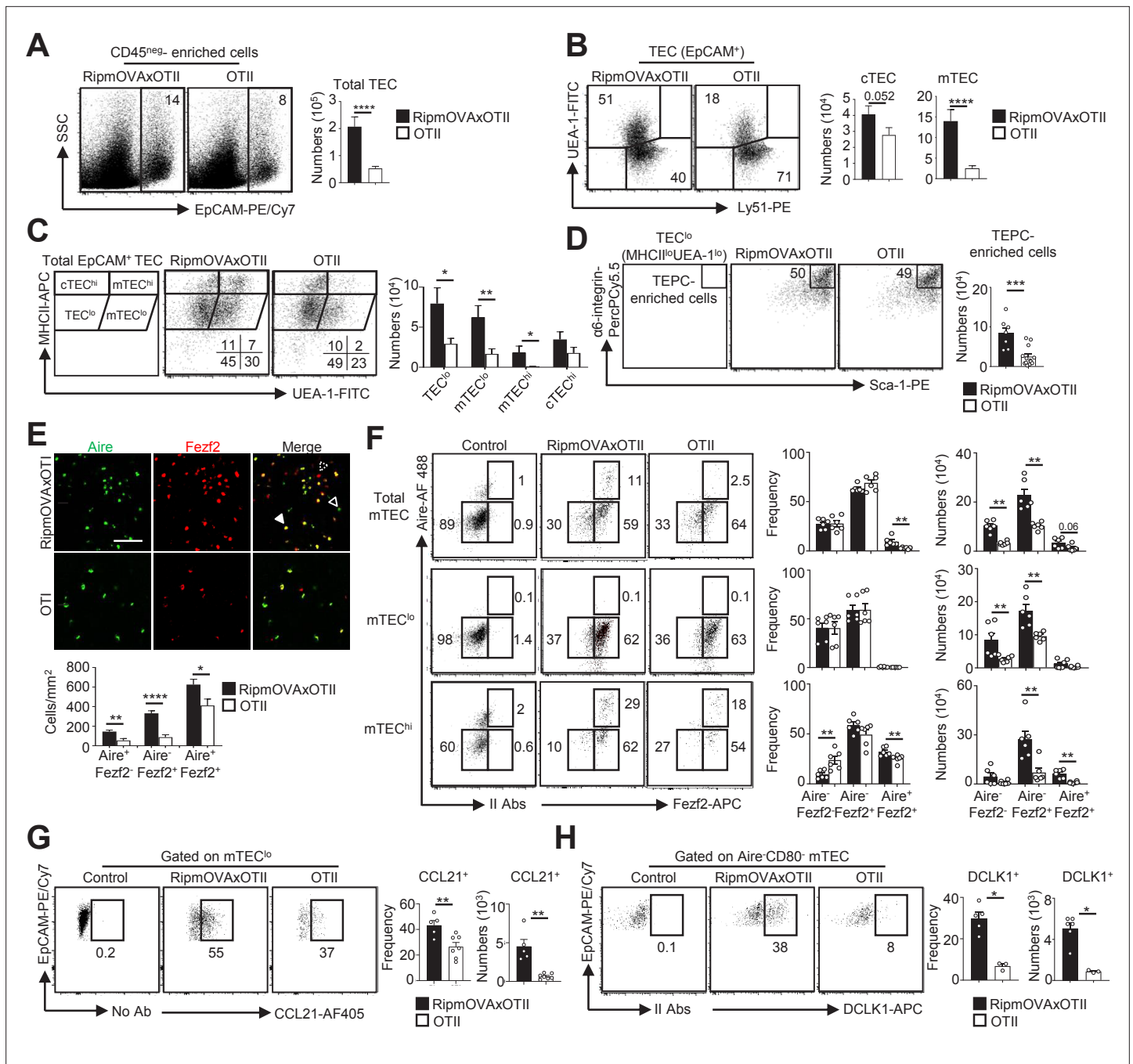


Figure 5. Highly self-reactive CD4⁺ thymocytes control medullary thymic epithelial cell (mTEC) development from an early progenitor stage. **(A–D)** Flow cytometry profiles and numbers of total thymic epithelial cells (TECs) (EpCAM⁺) **(A)**, cortical thymic epithelial cell (cTECs) (UEA-1⁺Ly51^{hi}), mTECs (UEA-1⁺Ly51^{lo}) **(B)**, TEC^{lo} (MHCII^{lo}UEA-1^{lo}), cTEC^{hi} (MHCII^{hi}UEA-1^{lo}), mTEC^{lo} (MHCII^{lo}UEA-1^{hi}), and mTEC^{hi} (MHCII^{hi}UEA-1^{hi}) **(C)**, α6-integrin^{hi}Sca-1^{hi} TEPC-enriched cells in TEC^{lo} **(D)** in CD45^{neg}-enriched cells from RipmOVAxOTII-Rag2^{-/-} and OTII-Rag2^{-/-} mice. Data are representative of four experiments (n = 3 mice per group and experiment). **(E)** Confocal images of thymic sections from RipmOVAxOTII-Rag2^{-/-} and OTII-Rag2^{-/-} mice stained for Aire (green) and Fezf2 (red). 11 and 22 sections derived from two RipmOVAxOTII-Rag2^{-/-} and OTII-Rag2^{-/-} mice were quantified, respectively. Scale bar, 50 μm. Unfilled, dashed and solid arrowheads indicate Aire⁺Fezf2^{lo}, Aire⁻Fezf2⁺, and Aire⁺Fezf2⁺ cells, respectively. The histogram shows the density of Aire⁺Fezf2^{lo}, Aire⁻Fezf2⁺, and Aire⁺Fezf2⁺ cells. **(F–H)** Flow cytometry profiles, frequencies, and numbers of Aire⁻Fezf2⁺, Aire⁺Fezf2⁺, and Aire⁺Fezf2^{lo} cells in total mTECs, mTEC^{lo}, and mTEC^{hi} **(F)**, of CCL21⁺ cells in mTEC^{lo} **(G)** and of DCLK1⁺ cells in Aire⁺ mTECs **(H)** from RipmOVAxOTII-Rag2^{-/-} and OTII-Rag2^{-/-} mice. II Abs: secondary antibodies. Data are representative of two independent experiments (n = 3–4 mice per group and experiment). Error bars show mean ± SEM, *p < 0.05, **p < 0.01, ***p < 0.001, ****p < 0.0001 using unpaired Student's t-test for **(A–E)** and two-tailed Mann–Whitney test for **(F–H)**.

The online version of this article includes the following figure supplement(s) for figure 5:

Figure 5 continued on next page

Figure 5 continued

Figure supplement 1. mTEC^{lo} and mTEC^{hi} cells are increased in RipmOVAxOTII-Rag2^{-/-} compared to OTII-Rag2^{-/-} mice.

Figure supplement 2. The proliferation of Aire⁺Fezf2⁺ and Aire⁺Fezf2⁺ medullary thymic epithelial cells (mTECs) is similar in RipmOVAxOTII-Rag2^{-/-} and OTII-Rag2^{-/-} mice.

Figure supplement 3. Post-Aire medullary thymic epithelial cells (mTECs) are increased in RipmOVAxOTII-Rag2^{-/-} compared to OTII-Rag2^{-/-} mice.

Self-reactive CD4⁺ thymocytes enhance the level of active H3K4me3 mark in mTEC^{lo}

Since histone modifications constitute important regulatory mechanisms that control the open and closed states of mTEC chromatin (Ucar and Rattay, 2015), we investigated whether self-reactive CD4⁺ thymocytes induce histone modifications in mTECs. We first analyzed in WT mTEC^{lo} the repressive H3K27me3 and the active H3K4me3 marks using chromatin immunoprecipitation (ChIP) followed by high-throughput sequencing (ChIP-seq). As expected, metagene analyses showed that Aire-dependent TRAs had higher levels of H3K27me3 in their genes than in all genes of the genome, confirming that they are in a repressive state (Figure 6A). In contrast, Fezf2-dependent TRAs had a significant enrichment of H3K4me3 in their transcriptional start site (TSS) (Figure 6B). Similarly, Aire/Fezf2-independent TRAs were associated with low levels of H3K27me3 in their genes and high levels of H3K4me3 in their TSS. Thus, in contrast to Aire-dependent TRAs that are associated with the repressive H3K27me3 histone mark, Fezf2-dependent and Aire/Fezf2-independent TRAs are associated with the active H3K4me3 mark, indicating that these distinct TRAs are subjected to a specific epigenetic regulation.

We next assessed whether highly self-reactive CD4⁺ thymocytes control the H3K27me3 and H3K4me3 chromatin landscape in mTEC^{lo}. In contrast to H3K27me3, we found an increased global level of H3K4me3 in RipmOVAxOTII-Rag2^{-/-} compared to OTII-Rag2^{-/-} mice by flow cytometry (Figure 6C). We further analyzed by nano-ChIP-seq whether self-reactive CD4⁺ thymocytes regulate in mTEC^{lo} the level of these two histone marks in Aire-dependent, Fezf2-dependent, and Aire/Fezf2-independent TRA genes. H3K27me3 levels in Aire-dependent TRA genes were comparable in mTEC^{lo} from RipmOVAxOTII-Rag2^{-/-} and OTII-Rag2^{-/-} mice (Figure 6D, left panel). Although lower, H3K27me3 levels in Fezf2-dependent and Aire/Fezf2-independent TRAs as well as in all genes were similar in both mice, indicating that the interactions with self-reactive CD4⁺ thymocytes do not regulate this repressive mark in TRA genes (Figure 6D, left panel). In contrast, H3K4me3 global level was increased in the TSS of all TRAs in RipmOVAxOTII-Rag2^{-/-} compared to OTII-Rag2^{-/-} mice as well as in all genes (Figure 6D, right panel). For representation, whereas the Aire/Fezf2-independent TRA, E2F transcription factor 2 (*E2f2*) induced by these interactions, was barely devoid of H3K27me3 in both mice, it was marked by H3K4me3 in its TSS specifically in RipmOVAxOTII-Rag2^{-/-} mice (Figure 6E). These results thus show that self-reactive CD4⁺ thymocytes enhance the global level of the active H3K4me3 histone mark in mTEC^{lo} and in particular in the TSS of Fezf2-dependent and Aire/Fezf2-independent TRAs, indicative of an epigenetic regulation for their expression.

MHCII/TCR interactions between mTECs and CD4⁺ thymocytes prevent the development of autoimmunity

We next evaluated the impact of mTEC-CD4⁺ thymocyte interactions on the generation of self-tolerant T cells by taking advantage that CD4⁺ and CD8⁺ T cells develop in mTEC^{ΔMHCII} mice, in which MHCII/TCR interactions between mTECs and CD4⁺ thymocytes are abrogated. Interestingly, since TRAs induced by MHCII/TCR interactions showed a diverse peripheral tissue distribution in mTEC^{lo} (Figure 7A, Supplementary file 4), we analyzed the TCRVβ usage in mTEC^{ΔMHCII} mice by flow cytometry. TCRVβ usage was more altered in CD69⁺ mature CD4⁺ thymocytes than in CD8⁺ thymocytes (Figure 7B). Some TCRVβ were also altered in splenic CD4⁺ and CD8⁺ T cells. To determine whether these T cells contained self-reactive specificities, we adoptively transferred splenocytes from mTEC^{ΔMHCII} or WT mice into lymphopenic Rag2^{-/-} recipients (Figure 7C). Mice that received splenocytes derived from mTEC^{ΔMHCII} mice lost significantly more weight than mice transferred with WT splenocytes (Figure 7D). They also exhibited splenomegaly with increased follicle areas and T-cell numbers showing a CD62L^{lo}CD44^{hi} effector and CD62L^{hi}CD44^{hi} central memory phenotype (Figure 7E–G). Immune infiltrates in lungs and salivary glands were observed by histology and flow cytometry in 75

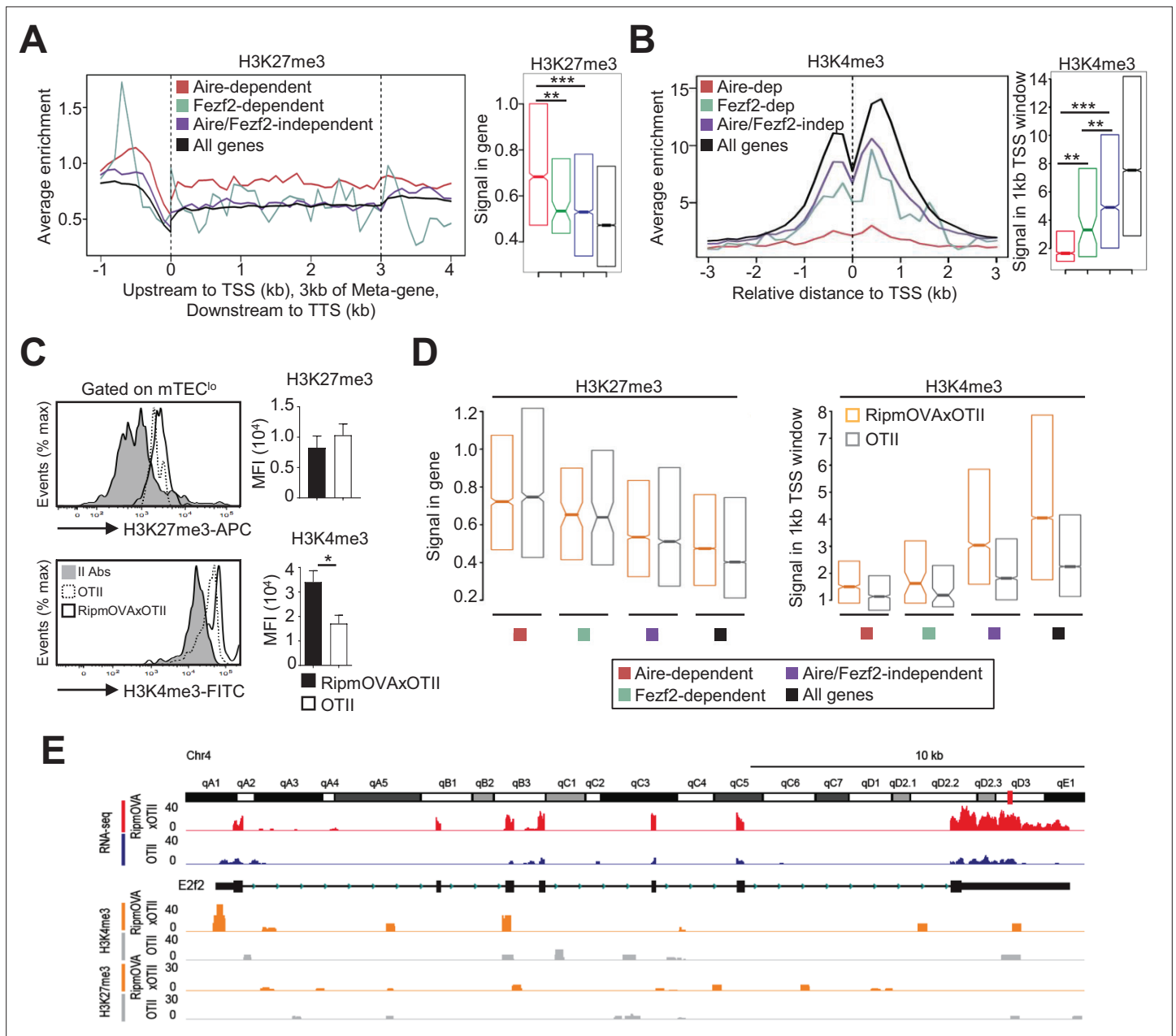


Figure 6. H3K27me3 and H3K4me3 landscape in tissue-restricted self-antigen (TRA) genes of mTEC^o from WT, RipmOVAxOTII-Rag2^{-/-}, and OTII-Rag2^{-/-} mice. **(A, B)** Metagene profiles of the average normalized enrichment of H3K27me3 **(A)** and H3K4me3 **(B)** against input for Aire-dependent, Fezf2-dependent, and Aire/Fezf2-independent TRAs as well as for all genes of WT mTEC^o. Boxplots represent the median enrichment, the 95% CI of the median (notches), and the 75th and 25th percentiles of H3K27me3 and H3K4me3. **(C)** H3K27me3 and H3K4me3 levels were analyzed by flow cytometry in mTEC^o from RipmOVAxOTII-Rag2^{-/-} (n = 4) and OTII-Rag2^{-/-} (n = 5) mice. Histograms show the MFI. **(D)** Boxplots represent the median enrichment of H3K27me3 and H3K4me3 of Aire-dependent, Fezf2-dependent, and Aire/Fezf2-independent TRAs and in all genes of mTEC^o from RipmOVAxOTII-Rag2^{-/-} and OTII-Rag2^{-/-} mice. **(E)** Expression (RNA-seq) and H3K27me3 and H3K4me3 chromatin state (ChIP-seq) of the Aire/Fezf2-independent TRA, E2f2, in mTEC^o from RipmOVAxOTII-Rag2^{-/-} and OTII-Rag2^{-/-} mice. *p<0.05, **p<10⁻³, ***p<10⁻⁷, using the Mann-Whitney test for **(A)** and **(B)** and unpaired Student's t-test for **(C)**.

and 41% of mice, respectively (**Figure 7H and I**). These two tissues contained increased numbers of central memory as well as CD44⁺CD69⁺ and CD44⁺CD69⁻ activated CD4⁺ and CD8⁺ T cells (**Figure 7J**). T-cell infiltrates were also observed in other tissues such as kidney, liver, and colon in agreement with the defective TRA expression associated with these tissues (**Figure 7A and K**). Altogether, these data show that in the absence of MHCII/TCR interactions between mTECs and CD4⁺ thymocytes, T cells

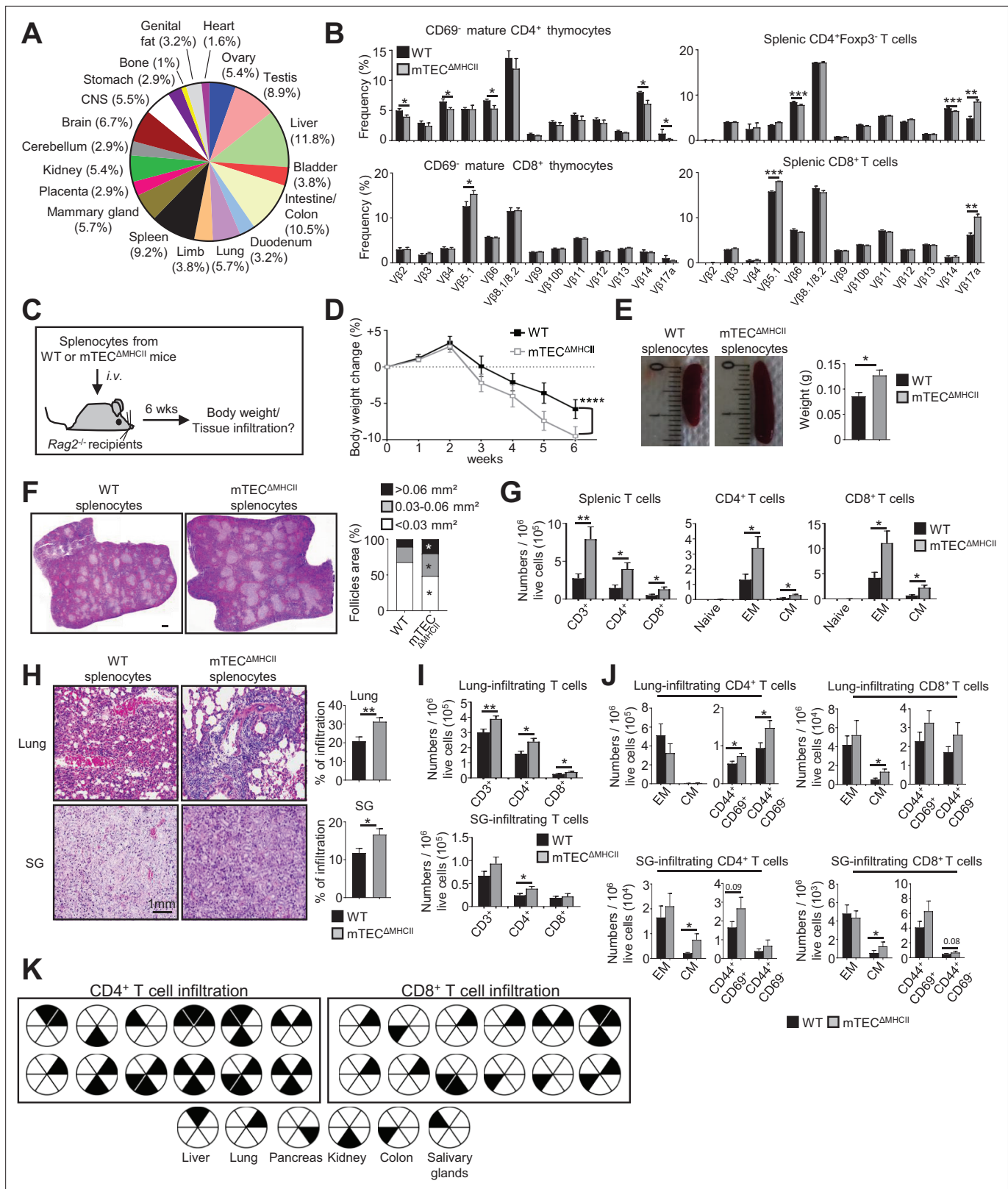


Figure 7. The adoptive transfer of T cells from mTEC Δ MHCII mice into Rag2^{-/-} recipients induces autoimmunity. (A) Tissue-restricted self-antigens (TRAs) underexpressed in mTEC^o from mTEC Δ MHCII mice were assigned to their peripheral expression. (B) TCR β usage by CD69⁺ mature CD4⁺ and CD8⁺ thymocytes (left panel) and CD4⁺Foxp3⁺ and CD8⁺ splenic T cells (right panel) from WT and mTEC Δ MHCII mice. (C) Body weight of Rag2^{-/-} recipients transferred with splenic T cells from WT or mTEC Δ MHCII was monitored during 6 weeks, and tissue infiltration was examined. (D) Weight loss relative

Figure 7 continued on next page

Figure 7 continued

to the initial weight. (E, F) Representative spleen pictures and their weights (E) and hematoxylin/eosin counterstained splenic sections (F). Scale bar, 1 mm. The histogram shows follicle areas. (G) Numbers of splenic CD3⁺, CD4⁺, and CD8⁺ T cells and of naive (CD44^{lo}CD62L^{hi}), effector memory (EM; CD44^{hi}CD62L^{lo}) and central memory (CM; CD44^{hi}CD62L^{hi}) phenotype. (H) Lung and salivary gland (SG) immune infiltrates detected by hematoxylin/eosin counterstaining. Scale bar, 1 mm. (I, J) Numbers of T cells (I) and of naive, effector and central memory phenotype as well as CD44⁺CD69⁺ and CD44⁺CD69⁻ T cells (J) in lungs and SG. (K) Schematic of T-cell infiltrates in mice transferred with mTEC^{ΔMHCII} T cells relative to those transferred with WT T cells. Each circle and black triangles represent an individual mouse and T-cell infiltration in a specific tissue, respectively. Data are representative of two independent experiments (n = 5–7 mice per group and experiment). Error bars show mean ± SEM, ****p<0.0001 using two-way ANOVA for (D) and unpaired Student's t-test for (B) and (E–J). *p<0.05, **p<0.01, ***p<0.001.

The online version of this article includes the following figure supplement(s) for figure 7:

Figure supplement 1. CD4⁺ thymocytes through MHCII/TCR-mediated interactions control transcriptional programs of mTEC^{lo} that drive their differentiation and function.

contained self-reactive specificities and thus that these interactions are critical to the establishment of T-cell tolerance.

Discussion

Since mTECs play a crucial role in immunological tolerance by their exclusive expression of TRAs, it is essential to deepen our knowledge of the mechanisms that sustain their differentiation. Here using three distinct transgenic models, we found that self-reactive CD4⁺ thymocytes control the developmental transcriptional programs from the mTEC^{lo} stage, including TAC-TECs that precede Aire⁺ mTECs. CD4⁺ thymocytes increase in mTEC^{lo} the phosphorylation of p38 MAPK and IKKα, the latter implicated in mTEC development (Lomada et al., 2007; Shen et al., 2019). Moreover, self-reactive CD4⁺ thymocytes increase RelB phosphorylation level. Interestingly, this nonclassical NF-κB subunit is crucial for mTEC differentiation and Aire-dependent and -independent TRA expression (Riemann et al., 2017). These data thus suggest that CD4⁺ thymocytes activate intracellular pathways from the mTEC^{lo} stage, although alterations in mTEC^{lo} subset composition could also contribute to the differences observed. Nevertheless, the substantial and homogeneous reduction in the levels of phospho-IKKα, -p38, and -RelB argues instead for impaired activation of IKKα, p38, and RelB signaling in the absence of self-reactive CD4⁺ thymocytes. Analysis of the mTEC^{lo} transcriptional landscape by high-throughput RNA-seq revealed that self-reactive CD4⁺ thymocytes upregulate *Nfkb2* (p52), known to form a heterocomplex with RelB in the nucleus upon activation (Irla et al., 2010). p52 is important for mTEC development, Aire, and TRA expression (Zhang et al., 2006; Zhu et al., 2006). Consequently, ΔCD4, mTEC^{ΔMHCII}, and OTII-*Rag2*^{-/-} mice in which MHCII/TCR interactions between mTECs and CD4⁺ thymocytes are disrupted have altered *Relb* and *Nfkb2* expression, and reduced Aire⁺ mTEC numbers and Aire-dependent TRA representation. Our results are in agreement with the fact that RANK-induced NF-κB signaling is activated by membrane-bound RANKL and not soluble RANKL and thereby in the context of physical interactions between mTECs and CD4⁺ thymocytes (Asano et al., 2019).

These interactions also upregulate *Trp53* (p53) that controls the mTEC niche (Rodrigues et al., 2017) and *Irf4* and *Irf7* transcription factors that regulate key chemokines implicated in thymocyte medullary localization and mTEC differentiation (Haljasorg et al., 2017; Otero et al., 2013). Furthermore, the deacetylase Sirtuin-1 (*Sirt1*), which regulates Aire activity (Chuprin et al., 2015), and *Spib*, which limits mTEC differentiation (Akiyama et al., 2014), were also upregulated. Self-reactive CD4⁺ thymocytes thus induce key transcription factors that both positively and negatively control mTEC differentiation. Remarkably, our three different transgenic models revealed that CD4⁺ thymocytes induce HDAC3-dependent mTEC-specific transcription factors (Goldfarb et al., 2016). Among them, *Pou2f3* is involved in tuft-like mTEC development (Bornstein et al., 2018; Miller et al., 2018), which is consistent with our results showing that self-reactive CD4⁺ thymocytes control the cellularity of these cells. Our data thus identify that CD4⁺ thymocytes control the expression of master transcriptional regulators of mTEC differentiation and function.

In line with these data, we found that self-reactive CD4⁺ thymocytes regulate TEC development from a progenitor stage since they increase numbers of TEPC-enriched cells that express non-negligible MHCII levels. Interestingly, we provide the first evidence that self-reactive CD4⁺ thymocytes

control the cellularity of Fezf2⁺ mTECs. Accordingly, the expression of Fezf2 and its respective TRAs was enhanced by CD4⁺ thymocytes. Moreover, self-reactive CD4⁺ thymocytes regulate the cellularity of CCL21⁺, post-Aire, and tuft-like cells in mTEC^{lo}. These results are in full agreement with our previous findings that self-reactive thymocytes drive medulla expansion and increase the overall cellularity of the mTEC compartment (Irla et al., 2012). Because the heterogeneous composition in mTEC^{lo} could influence the expression of the upregulated genes by self-reactive CD4⁺ thymocytes, we reanalyzed single-cell RNA-seq data in order to define their respective expression pattern in mTEC subsets. In accordance with the moderately altered frequencies of CCL21⁺ cells among mTEC^{lo} observed by flow cytometry, few genes upregulated by self-reactive CD4⁺ thymocytes were associated with this mTEC subset. In contrast, we found that antigen-specific interactions with CD4⁺ thymocytes strongly upregulate genes associated with TAC-TECs, Aire⁺ mTECs, and post-Aire cells. These findings indicate that self-reactive CD4⁺ thymocytes act from the precursors of Aire⁺ mTEC^{hi} (i.e., in TAC-TECs) to the post-Aire stage. It is interesting to note that although strongly altered the development of mTEC^{hi} is not completely abrogated in the absence of CD4⁺ thymocytes or MHCII/TCR-mediated interactions with CD4⁺ thymocytes. This could be explained by the fact that invariant NKT have been proposed to participate in mTEC differentiation by expressing RANKL (White et al., 2014). Overall, our results thus reveal that antigen-specific interactions with CD4⁺ thymocytes have an unsuspected broad impact on mTEC composition by driving their development from an early progenitor to a late post-Aire stage.

Interestingly, high-throughput RNA-seq showed that MHCII/TCR interactions with CD4⁺ thymocytes upregulate the expression of chemokines in mTEC^{lo}. Among them, CCL19 (CCR7 ligand) is implicated in the medullary localization of thymocytes and the emigration of newly generated T cells (Ueno et al., 2004); and CCL22 (CCR4 ligand) implicated in medullary entry and thymocyte/dendritic cell interactions (Hu et al., 2015). Self-reactive CD4⁺ thymocytes also enhance CCL2 (CCR2 ligand) and CCL20 (CCR6 ligand) that promote the entry of peripheral dendritic cells and Foxp3⁺ regulatory T cells into the thymus (Baba et al., 2009; Cédile et al., 2014; Cowan et al., 2018; Lopes et al., 2018; Borelli and Irla, 2021). mTEC-CD4⁺ thymocyte interactions thus induce key chemokines that regulate the trafficking of thymocytes and dendritic cells that participate in tolerance induction. Moreover, cytokines such as *Il15* and *Fgf21* implicated in invariant NKT development and TEC protection against senescence, as well as adhesion molecules involved in mTEC-thymocyte interactions, were also induced (Pezzi et al., 2016; White et al., 2014; Youm et al., 2016). Altogether, our data show that self-reactive CD4⁺ thymocytes regulate functional properties of mTECs by inducing chemokines, cytokines, and adhesion molecules that are critical for T-cell development.

The expression of TRAs is regulated by Aire and to a lesser extent by Fezf2 (Anderson et al., 2002; Takaba et al., 2015). In agreement with other studies (Gray et al., 2007; Takaba et al., 2015), we found Fezf2 in both mTEC^{lo} and mTEC^{hi}, whereas Aire protein is mainly expressed in mTEC^{hi}. Nevertheless and in line with recent single-cell transcriptomic analyses (Baran-Gale et al., 2020; Dhalla et al., 2020; Wells et al., 2020), we detected Aire by flow cytometry, qPCR, and RNA-seq in a small subset (~1.5%) of mTEC^{lo}. CD4⁺ thymocyte interactions upregulate *Aire* and *Fezf2* and some of their respective TRAs in these cells. Interestingly, in contrast to Aire-dependent TRAs that are characterized by high levels of H3K27me3 (Handel et al., 2018; Sansom et al., 2014), we found that Fezf2-dependent TRAs show high levels of H3K4me3. This highlights that Aire and Fezf2 use distinct epigenetic modes in regulating TRA expression. Remarkably, these interactions also induce in mTEC^{lo} numerous Aire/Fezf2-independent TRAs, whose regulation remains unknown. Similarly to Fezf2-dependent TRAs, they had high levels of H3K4me3 in their TSS, suggesting that Aire/Fezf2-independent TRAs are not subjected to the same regulatory transcriptional mechanisms than Aire-dependent TRAs. Our results are consistent with a previous study indicating that the Aire-independent TRA, *Gad1*, shows active epigenetic marks (Tykocinski et al., 2010). Remarkably, self-reactive CD4⁺ thymocytes increase H3K4me3 level in the TSS of all TRA categories, thus providing a novel epigenetic mechanistic insight into how they regulate the mTEC gene expression profile. In line with TRA regulation and the development of distinct mTEC subsets, the repertoire of mature T cells contains autoreactive cells when MHCII/TCR interactions were abrogated between mTECs and CD4⁺ thymocytes. Accordingly, the adoptive transfer of splenocytes from mTEC^{ΔMHCII} mice is capable of inducing signs of autoimmunity, illustrating the fact that mTEC-CD4⁺ thymocyte interactions are critical for the generation of a self-tolerant T-cell repertoire. Future investigations based on TCR sequencing analysis are expected to define to which extent the TCR repertoire is altered in mTEC^{ΔMHCII} mice.

In summary, our genome-wide scale study reveals that self-reactive CD4⁺ thymocytes activate transcriptional programs from the TAC-TEC stage that sustains the differentiation into Aire⁺Fezf2⁺ and post-Aire mTECs (**Figure 7—figure supplement 1**). These interactions also upregulate the expression of TRAs, cytokines, chemokines, and adhesion molecules that are all implicated in mTEC function. Thus, CD4⁺ thymocytes control several unsuspected aspects of mTEC^{lo} required for the establishment of T-cell tolerance.

Materials and methods

Key resources table

Reagent type (species) or resource	Designation	Source or reference	Identifiers	Additional information
Genetic reagent (<i>Mus musculus</i>)	C57BL/6J background	Charles River	RRID:IMSR_JAX:000664	
Genetic reagent (<i>M. musculus</i>)	<i>Ciita</i> ^{tm2Wrth} / <i>Ciita</i> ^{tm2Wrth}	LeibundGut-Landmann et al., 2004	RRID:MGI:3052466	C57BL/6 background, ΔCD4 mice
Genetic reagent (<i>M. musculus</i>)	H2 ^{dIAb1-Ea} /H2 ^{dIAb1-Ea}	Madsen et al., 1999	RRID:MGI:4436873	C57BL/6 background, MHCII ^{-/-} mice
Genetic reagent (<i>M. musculus</i>)	K14x <i>Ciita</i> ^{III+IV-/-}	Irla et al., 2008		C57BL/6 background, mTEC ^{ΔMHCII} mice
Genetic reagent (<i>M. musculus</i>)	Tg(TcraTcrb)425Cbn	Barnden et al., 1998	RRID:MGI:3762632	C57BL/6 background, OTII mice
Genetic reagent (<i>M. musculus</i>)	Tg(Ins2-TFRC/OVA)296Wehi	Kurts et al., 1996	RRID:MGI:3623748	C57BL/6 background, Rip-mOVA mice
Genetic reagent (<i>M. musculus</i>)	<i>Rag2</i> ^{tm1Fwa} / <i>Rag2</i> ^{tm1Fwa}	Shinkai et al., 1992	RRID:MGI:2174910	C57BL/6 background, <i>Rag2</i> ^{-/-} mice
Antibody	Anti-IKKα (rabbit polyclonal)	Cell Signaling Technology	Cat# 2682; RRID:AB_331626	FACS (1:500)
Antibody	Anti-phospho IKKα (Ser180)/IKKβ(Ser181) (rabbit polyclonal)	Cell Signaling Technology	Cat# 2681S; RRID:AB_331624	FACS (1:500)
Antibody	Anti-p38 MAPK (rabbit polyclonal)	Cell Signaling Technology	Cat# 9212; RRID:AB_330713	FACS (1:500)
Antibody	Anti-phospho p38 MAPK (Thr180/Tyr182) (rabbit polyclonal)	Cell Signaling Technology	Cat# 9211S; RRID:AB_331641	FACS (1:500)
Antibody	Anti-Erk1/2 (rabbit polyclonal)	Cell Signaling Technology	Cat# 9102; RRID:AB_330744	FACS (1:500)
Antibody	Anti-phospho Erk1/2 (Thr202/Tyr204) (rabbit polyclonal)	Cell Signaling Technology	Cat# 9101S; RRID:AB_331646	FACS (1:500)
Antibody	Anti-NF-κB p65 (clone D14E12, rabbit monoclonal)	Cell Signaling Technology	Cat# 8242S; RRID:AB_10859369	FACS (1:500)
Antibody	Phospho-NF-κB p65 (Ser536) (clone 93H1, rabbit monoclonal)	Cell Signaling Technology	Cat# 3033S; RRID:AB_331284	FACS (1:3000)
Antibody	Anti-RelB (clone C-19, rabbit polyclonal)	Santa Cruz Biotechnology	Cat# sc-226; RRID:AB_632341	FACS (1:200)
Antibody	Anti-phospho RelB (ser552) (clone D41B9, rabbit monoclonal)	Cell Signaling Technology	Cat# 5025S; RRID:AB_10622001	FACS (1:1000)
Antibody	Anti-DCLK1 (clone D2U3L, rabbit monoclonal)	Cell Signaling Technology	Cat# 62257; RRID:AB_2799622	FACS (1:200)
Antibody	Anti-H3K4me3 (rabbit polyclonal)	Abcam	Cat# ab8580; RRID:AB_306649	FACS (1:1000) ChIP-seq (2 μg:25 μg chromatin)
Antibody	Anti-H3K27me3 (clone C36B11, rabbit monoclonal)	Cell Signaling Technology	Cat# 9733; RRID:AB_2616029	FACS (1:1000) ChIP-seq (1:50)

Continued on next page

Continued

Reagent type
(species) or
resource

Reagent type (species) or resource	Designation	Source or reference	Identifiers	Additional information
Antibody	PE-Cy7 anti-CD326 (EpCAM) (clone G8.8, rat monoclonal)	eBioscience	Cat# 25-5791-80; RRID:AB_1724047	FACS (1:3000)
Antibody	Alexa Fluor 488 anti-Aire (clone 5H12, rat monoclonal)	eBioscience	Cat# 53-5934-82; RRID:AB_10854132	FACS, IF (1:200)
Antibody	PE anti-Ly51 (clone BP-1, mouse monoclonal)	BD Biosciences	Cat# 553735; RRID:AB_395018	FACS (1:3000)
Antibody	PerCP-Cy5.5 anti-CD80 (clone 16-10A1, Armenian hamster monoclonal)	BioLegend	Cat# 104722; RRID:AB_2291392	FACS (1:200)
Antibody	eFluor 450 anti-Ki-67 (clone SolA15, rat monoclonal)	eBioscience	Cat# 48-5698-82; RRID:AB_11149124	FACS (1:200)
Antibody	Anti-Fezf2 (clone F441, rabbit polyclonal)	IBL Tecan	Cat# JP18997; RRID:AB_2341444	FACS, IF (1:200)
Antibody	Anti-Involucrin (clone Poly19244, rabbit polyclonal)	BioLegend	Cat# 924401; RRID:AB_2565452	IF (1:100)
Antibody	PE anti-Ly-6A/E (Sca-1) (clone D7, rat monoclonal)	BD Biosciences	Cat# 553108; RRID:AB_394629	FACS (1:600)
Antibody	Biotin anti-CD49f ($\alpha 6$ -integrin) (clone GoH3, rat monoclonal)	BioLegend	Cat# 313604; RRID:AB_345298	FACS (1:200)
Antibody	Alexa Fluor 647 anti-I-Ab (MHCII) (clone AF6-120.1, mouse monoclonal)	BioLegend	Cat# 116412; RRID:AB_493141	FACS (1:200)
Antibody	Brilliant Violet 421 anti-CD4 (clone RM4-5, rat monoclonal)	BioLegend	Cat# 100544; RRID:AB_11219790	FACS (1:200)
Antibody	PerCP-Cy5.5 anti-CD4 (clone RM4-5, rat monoclonal)	BD Biosciences	Cat# 550954; RRID:AB_393977	FACS (1:200)
Antibody	Pacific Blue anti-CD8 α (clone 53-6.7, rat monoclonal)	BD Biosciences	Cat# 558106; RRID:AB_397029	FACS (1:200)
Antibody	PE/Cy7 anti-CD8 α (clone 53-6.7, rat monoclonal)	BioLegend	Cat# 100722; RRID:AB_312761	FACS (1:600)
Antibody	Alexa Fluor 488 anti-CD44 (clone IM7, rat monoclonal)	BioLegend	Cat# 103016; RRID:AB_493679	FACS (1:200)
Antibody	PE anti-CD69 (clone H1.2F3, rat monoclonal)	BioLegend	Cat# 104508; RRID:AB_313111	FACS (1:400)
Antibody	PE anti-CD62L (clone MEL-14, rat monoclonal)	BD Biosciences	Cat# 553151; RRID:AB_394666	FACS (1:300)
Antibody	PerCP-Cy5.5 anti-CD3 ϵ (clone 17A2, rat monoclonal)	BD Biosciences	Cat# 560527; RRID:AB_1727463	FACS (1:200)
Antibody	Alexa Fluor 405 anti-CCL21 (clone 59106, rat monoclonal)	R&D Systems	Cat# IC457V	FACS (1:100)
Antibody	CD45 MicroBeads, mouse (clone 30F11.1, rat monoclonal)	Miltenyi	Cat# 130052301; RRID:AB_2877061	
Antibody	Cy5 anti-rabbit IgG (goat polyclonal)	Invitrogen	Cat# A10523; RRID:AB_2534032	FACS (1:500)
Antibody	Cyanine 3 anti-rabbit IgG (goat polyclonal)	Invitrogen	Cat# A10520; RRID:AB_2534029	IF (1:500)
Antibody	FITC anti-TCR V β 2 (clone B20.6, rat monoclonal)	BD Biosciences	Cat# 557004; RRID:AB_647180	FACS (20 μ l per 10 ⁶ cells)
Antibody	FITC anti-TCR V β 3 (clone KJ25, Armenian hamster monoclonal)	BD Biosciences	Cat# 557004; RRID:AB_647180	FACS (20 μ l per 10 ⁶ cells)

Continued on next page

Continued

Reagent type (species) or resource	Designation	Source or reference	Identifiers	Additional information
Antibody	FITC anti-TCR V β 4 (clone KT4, rat monoclonal)	BD Biosciences	Cat# 557004; RRID:AB_647180	FACS (20 μ l per 10 ⁶ cells)
Antibody	FITC anti-TCR V β 5.1, 5.2 (clone MR9-4, mouse monoclonal)	BD Biosciences	Cat# 553189; RRID:AB_394697	FACS (1:100)
Antibody	FITC anti-TCR V β 6 (clone RR4-7, rat monoclonal)	BD Biosciences	Cat# 557004; RRID:AB_647180	FACS (20 μ l per 10 ⁶ cells)
Antibody	PE anti-TCR V β 8.1, 8.2 (clone MR5-2, mouse monoclonal)	BioLegend	Cat# 140103; RRID:AB_10641144	FACS (1:300)
Antibody	FITC anti-TCR V β 9 (clone MR10-2, mouse monoclonal)	BD Biosciences	Cat# 557004; RRID:AB_647180	FACS (20 μ l per 10 ⁶ cells)
Antibody	PE anti-TCR V β 10b (clone B21.5, rat monoclonal)	BD Biosciences	Cat# 553285; RRID:AB_394757	FACS (1:300)
Antibody	Biotin anti-TCR V β 11 (clone RR3-15, rat monoclonal)	BD Biosciences	Cat# 553196; RRID:AB_394702	FACS (1:300)
Antibody	FITC anti-TCR V β 12 (clone MR11-1, mouse monoclonal)	BD Biosciences	Cat# 557004; RRID:AB_647180	FACS (20 μ l per 10 ⁶ cells)
Antibody	FITC anti-TCR V β 13 (clone MR12-3, mouse monoclonal)	BD Biosciences	Cat# 557004; RRID:AB_647180	FACS (20 μ l per 10 ⁶ cells)
Antibody	FITC anti-TCR V β 14 (clone 14-2, rat monoclonal)	BD Biosciences	Cat# 557004; RRID:AB_647180	FACS (20 μ l per 10 ⁶ cells)
Antibody	FITC anti-TCR V β 17a (clone KJ23, rat monoclonal)	BD Biosciences	Cat# 557004; RRID:AB_647180	FACS (20 μ l per 10 ⁶ cells)
Antibody	CD4 ⁺ T cell isolation kit, mouse	Miltenyi Biotec	Cat# 130-104-454	
Peptide, recombinant protein	PerCP-Cy5.5 Streptavidin	BioLegend	Cat# 405214; RRID:AB_2716577	FACS (1:400)
Peptide, recombinant protein	Alexa Fluor 488 Streptavidin	Invitrogen	Cat# S11223	IF (1:1000)
Peptide, recombinant protein	Ovalbumin (323–339)	PolyPeptide	Cat# SC1303	5 μ M
Chemical compound, drug	Liberase TM	Roche	Cat# 05401127001	50 μ g/ml
Chemical compound, drug	DNase I	Roche	Cat# 10104159001	100 μ g/ml
Chemical compound, drug	TRIzol	Thermo Fisher Scientific	Cat# 15596018	
Software, algorithm	GraphPad Prism	GraphPad Software	RRID:SCR_002798	
Software, algorithm	FlowJo	FlowJo	https://www.flowjo.com/ RRID:SCR_008520	
Software, algorithm	Fiji/ImageJ software	Fiji-ImageJ	https://imagej.nih.gov/ij/ RRID:SCR_003070	
Software, algorithm	7500 Real-Time PCR Software	Thermo Fisher	https://www.thermofisher.com/us/en/home/technical-resources/software-downloads/applied-biosystems-7500-real-time-pcr-system.html RRID:SCR_014596	
Software, algorithm	Pheatmap 0.2	https://github.com/raivokolde/pheatmap (Kolde, 2018)	RRID:SCR_016418	
Software, algorithm	Seurat	Hao et al., 2021	RRID:SCR_016341	

Continued on next page

Continued

Reagent type (species) or resource	Designation	Source or reference	Identifiers	Additional information
Sequence-based reagent	Actin-FW	Sigma-Aldrich	PCR primers	CAGAAGGAGATTACTGCTCTGGCT
Sequence-based reagent	Actin-RV	Sigma-Aldrich	PCR primers	GGAGCCACCGATCCACACA
Sequence-based reagent	Aire-FW	Sigma-Aldrich	PCR primers	GCATAGCATCCTGGACGGCTTCC
Sequence-based reagent	Aire-RV	Sigma-Aldrich	PCR primers	CTGGGCTGGAGACGCTCTTTGAG
Sequence-based reagent	Ccl19-FW	Sigma-Aldrich	PCR primers	GCTAATGATGCGGAAGACTG
Sequence-based reagent	Ccl19-RV	Sigma-Aldrich	PCR primers	ACTCACATCGACTCTCTAGG
Sequence-based reagent	Ccl2-FW	Sigma-Aldrich	PCR primers	TGGAGCATCCACGTGTTG
Sequence-based reagent	Ccl2-RV	Sigma-Aldrich	PCR primers	ACTCATTGGGATCATCTTGCT
Sequence-based reagent	Ccl22-FW	Sigma-Aldrich	PCR primers	CTGATGCAGGTCCTATGGT
Sequence-based reagent	Ccl22-RV	Sigma-Aldrich	PCR primers	GGAGTAGCTTCTTACCCAG
Sequence-based reagent	Ccl25-FW	Sigma-Aldrich	PCR primers	GCCTGGTTGCCTGTTTTGTT
Sequence-based reagent	Ccl25-RV	Sigma-Aldrich	PCR primers	ACCCAGGCAGCAGTCTTCAA
Sequence-based reagent	Cdh2-FW	Sigma-Aldrich	PCR primers	AGCGCAGTCTTACCGAAGG
Sequence-based reagent	Cdh2-RV	Sigma-Aldrich	PCR primers	TCGCTGCTTTCATACTGAACCTT
Sequence-based reagent	Coch-FW	Sigma-Aldrich	PCR primers	GTGAGCAAAACCTGCTACAA
Sequence-based reagent	Coch -RV	Sigma-Aldrich	PCR primers	AGCTAGGACGTTCTCTTTGGT
Sequence-based reagent	Crabp1-FW	Sigma-Aldrich	PCR primers	CAGCAGCGAGAATTCGACGA
Sequence-based reagent	Crabp1-RV	Sigma-Aldrich	PCR primers	CGCACAGTAGTGGATGTCTTGA
Sequence-based reagent	Crp-FW	Sigma-Aldrich	PCR primers	CATAGCCATGGAGAAGCTAC
Sequence-based reagent	Crp-RV	Sigma-Aldrich	PCR primers	CAGTGGCTTCTTTGACTCTG
Sequence-based reagent	Csn2-FW	Sigma-Aldrich	PCR primers	CTCCACTAAAGGACTTGACAG
Sequence-based reagent	Csn2-RV	Sigma-Aldrich	PCR primers	ACCTTCTGAAGTTTCTGCTC
Sequence-based reagent	Fabp9-FW	Sigma-Aldrich	PCR primers	CACTGCAGACAACCGAAAAG
Sequence-based reagent	Fabp9-RV	Sigma-Aldrich	PCR primers	TCTGTTTGCCAAGCCATTTT
Sequence-based reagent	Fam183b-FW	Sigma-Aldrich	PCR primers	CGTGTGGGGCAGATGAAGAAT

Continued on next page

Continued

Reagent type (species) or resource	Designation	Source or reference	Identifiers	Additional information
Sequence-based reagent	Fam183b-RV	Sigma-Aldrich	PCR primers	GGTGAATGAGGTTGAGGAACTTG
Sequence-based reagent	Fcer2a-FW	Sigma-Aldrich	PCR primers	CCAGGAGGATCTAAGGAACGC
Sequence-based reagent	Fcer2a-RV	Sigma-Aldrich	PCR primers	TCGTCTGGAGTCTGTTGAGG
Sequence-based reagent	Fezf2-FW	Sigma-Aldrich	PCR primers	CAGCACTCTCTGCAGACACAA
Sequence-based reagent	Fezf2-RV	Sigma-Aldrich	PCR primers	TGCCGCACTGGTTACTACTTA
Sequence-based reagent	Grap-FW	Sigma-Aldrich	PCR primers	GATCAGGGAGAGTGAGAGTTCC
Sequence-based reagent	Grap-RV	Sigma-Aldrich	PCR primers	CAGCTCGTTGAGGGAGTTGA
Sequence-based reagent	Icam2-FW	Sigma-Aldrich	PCR primers	ATCAACTGCAGCACCAACTG
Sequence-based reagent	Icam2-RV	Sigma-Aldrich	PCR primers	ACTTGAGCTGGAGGCTGGTA
Sequence-based reagent	Il15-FW	Sigma-Aldrich	PCR primers	AGCAGATAACCAGCCTACAGGA
Sequence-based reagent	Il15-RV	Sigma-Aldrich	PCR primers	TGTTGAAGATGAGCTGGCTATGG
Sequence-based reagent	Il21-FW	Sigma-Aldrich	PCR primers	CGCCTCTGATTAGACTTCG
Sequence-based reagent	Il21-RV	Sigma-Aldrich	PCR primers	TGGAGCTGATAGAAGTTCAGGA
Sequence-based reagent	Il5-FW	Sigma-Aldrich	PCR primers	CCGCCAAAAGAGAAGTGTGGCGA
Sequence-based reagent	Il5-RV	Sigma-Aldrich	PCR primers	GCCTCAGCCTCCATTGCCCA
Sequence-based reagent	Il7-FW	Sigma-Aldrich	PCR primers	GGGTCTGGGAGTGATTATGG
Sequence-based reagent	Il7-RV	Sigma-Aldrich	PCR primers	CGGGAGGTGGGTGTAGTCAT
Sequence-based reagent	Itgad-FW	Sigma-Aldrich	PCR primers	CGAAAGGGTTCAGACTTTGC
Sequence-based reagent	Itgad-RV	Sigma-Aldrich	PCR primers	ACACCTCCACGGATAGAAGTC
Sequence-based reagent	Itgb6-FW	Sigma-Aldrich	PCR primers	GCTGGTCTGCCTGTTTCTGC
Sequence-based reagent	Itgb6-RV	Sigma-Aldrich	PCR primers	TGAGCAGCTTTCTGCACCAC
Sequence-based reagent	Kcnj5-FW	Sigma-Aldrich	PCR primers	AAAACCTTAGCGGCTTTGTATCT
Sequence-based reagent	Kcnj5-RV	Sigma-Aldrich	PCR primers	AAGGCATTAACAATCGAGCCC
Sequence-based reagent	Krt1-FW	Sigma-Aldrich	PCR primers	TGGGAGATTTTCAGGAGGAGG
Sequence-based reagent	Krt1-RV	Sigma-Aldrich	PCR primers	GCCCACTCTTGAGATGCTC

Continued on next page

Continued

Reagent type (species) or resource	Designation	Source or reference	Identifiers	Additional information
Sequence-based reagent	Meig1-FW	Sigma-Aldrich	PCR primers	CTTCAGCGGAGGGACAATAC
Sequence-based reagent	Meig1-RV	Sigma-Aldrich	PCR primers	CAAGGTTTCAAGGTGGGTGT
Sequence-based reagent	Nov-FW	Sigma-Aldrich	PCR primers	AGACCCCAACAACCAGACTG
Sequence-based reagent	Nov-RV	Sigma-Aldrich	PCR primers	CGGTAAATGACCCCATCGAAC
Sequence-based reagent	Nts-FW	Sigma-Aldrich	PCR primers	GCAAGTCCTCCGCTTGGAAA
Sequence-based reagent	Nts-RV	Sigma-Aldrich	PCR primers	TGCCAACAAGGTCGTCATCAT
Sequence-based reagent	Reig1-FW	Sigma-Aldrich	PCR primers	ATGGCTAGGAACGCCTACTTC
Sequence-based reagent	Reig1-RV	Sigma-Aldrich	PCR primers	CCCAAGTTAAACGGTCTTCAGT
Sequence-based reagent	Resp18-FW	Sigma-Aldrich	PCR primers	CCAGCCAAGATGCAGAGTTCGTTAAAG
Sequence-based reagent	Resp18-RV	Sigma-Aldrich	PCR primers	TCAGTCAGCAACAAGGTTGAGGCCAC
Sequence-based reagent	Rsph1-FW	Sigma-Aldrich	PCR primers	ACGGGGACACATATGAAGGA
Sequence-based reagent	Rsph1-RV	Sigma-Aldrich	PCR primers	GGCCGTGCTTTTTATTTTTG
Sequence-based reagent	Spon2-FW	Sigma-Aldrich	PCR primers	ATGGAAAACGTGAGTCTTGCC
Sequence-based reagent	Spon2-RV	Sigma-Aldrich	PCR primers	TGATGCTGTATCTAGCCAGAGG
Sequence-based reagent	Sult1c2-FW	Sigma-Aldrich	PCR primers	ATGGCCTTGACCCAGAAC
Sequence-based reagent	Sult1c2-RV	Sigma-Aldrich	PCR primers	TCGAAGGTCTGAATCTGCCTC
Sequence-based reagent	Upk3b-FW	Sigma-Aldrich	PCR primers	CATCTGGCTAGTGGTGGCTTT
Sequence-based reagent	Upk3b-RV	Sigma-Aldrich	PCR primers	GGTAATGTCATATAGTGGCCGTC
Other	Biotinylated Lotus Tetragonolobus Lectin (LTL)	Vector Laboratories	Cat# B-1325; RRID:AB_2336558	IF (1:500)
Other	FITC Ulex Europaeus Agglutinin I (UEA I)	Vector Laboratories	Cat# FL-1061; RRID:AB_2336767	FACS (1:600)
Other	SuperScript II Reverse Transcriptase	Thermo Fisher	Cat# 18064022	
Other	SYBR Premix Ex Taq master mix	Takara	Cat# RR390A	
Other	miRNeasy Micro Kit	QIAGEN	Cat# 217084	
Other	TruSeq ChIP Library Preparation Kit	Illumina	Cat# IP-202-2012	

Mice

C57BL/6 WT mice were purchased from Charles River. *Ciita*^{III+IV-/-} (Δ CD4) (LeibundGut-Landmann et al., 2004), *MHCII*^{-/-} (Madsen et al., 1999), *K14xCiita*^{III -/-} (*mTEC* ^{Δ MHCII}) (Irla et al., 2008), *OTII* (Barnden et al., 1998), *RipmOVAxOTII* (Kurts et al., 1996), and *Rag2*^{-/-} (Shinkai et al., 1992) mice were on C57BL/6J background. *OTII* and *RipmOVAxOTII* were backcrossed on *Rag2*^{-/-} background. All mice were maintained under specific pathogen-free conditions at an ambient temperature of 22°C at

the animal facilities of the CIML (Marseille, France). Standard food and water were given ad libitum. Males and females were used at the age of 5–6 weeks. All experiments were done in accordance with national and European laws for laboratory animal welfare (EEC Council Directive 2010/63/UE), and were approved by the Marseille Ethical Committee for Animal Experimentation (Comité National de Réflexion Ethique sur l'Expérimentation Animale no. 14).

mTEC purification

mTECs were isolated by enzymatic digestion with 50 µg/ml of Liberase TM (Roche) and 100 µg/ml of DNase I (Roche) in HBSS medium, as previously described (Lopes et al., 2017). CD45⁺ hematopoietic cells were depleted using anti-CD45 magnetic beads by autoMACS with the depleteS program (Miltenyi Biotec). Total mTECs (EpCAM⁺UEA-1⁺Ly51^{lo}), mTEC^{lo} (EpCAM⁺UEA-1⁺Ly51^{lo}CD80^{lo/int}), and mTEC^{hi} (EpCAM⁺UEA-1⁺Ly51^{lo}CD80^{hi}) were sorted with a FACSAriaIII cell sorter (BD). The purity of sorted mTEC^{lo} was >98%. Flow cytometry gating strategies are shown in **Figure 1—figure supplement 1**.

mTEC antigen presentation assays

Variable numbers of mTECs from WT and mTEC^{ΔMHCII} mice loaded or not with OVA₃₂₃₋₃₃₉ (5 µM, Polypeptide group) were co-cultured with 10⁵ OTII CD4⁺ T cells (purified with a CD4⁺ T cell isolation kit, Miltenyi Biotec) in RPMI medium (Thermo Fisher) supplemented with 10% FCS (Sigma-Aldrich), L-glutamine (2 mM, Thermo Fisher), sodium pyruvate (1 mM, Thermo Fisher), 2-mercaptoethanol (2 × 10⁻⁵ M, Thermo Fisher), penicillin (100 IU/ml, Thermo Fisher), and streptomycin (100 µg/ml, Thermo Fisher). The activation of OTII CD4⁺ T cells was assessed 18 hr later by flow cytometry based on the upregulation of the CD69 marker.

Flow cytometry

TECs, thymocytes, and splenic T cells were analyzed by flow cytometry (FACSCanto II, BD) with standard procedures. Cells were incubated for 15 min at 4°C with Fc-block (anti-CD16/CD32, 2.4G2, BD Biosciences) before staining. Antibodies are listed in the Key resources table. For intracellular staining with anti-Foxp3, anti-Ki-67, anti-p38 MAPK, anti-phospho p38 MAPK (Thr180/Tyr182), anti-IKKα, anti-phospho IKKα(Ser180)/IKKβ(Ser181), anti-Erk1/2 MAPK, anti-phospho Erk1/2 MAPK (Thr202/Tyr204), anti-p65, anti-phospho p65(ser536), anti-RelB, anti-phospho RelB(ser552), and anti-DCLK1 antibodies, cells were fixed, permeabilized, and stained with the Foxp3 staining kit according to the manufacturer's instructions (eBioscience). Intracellular staining with anti-Aire, anti-Fezf2, anti-CCL21, anti-H3K4me3, and anti-H3K27me3 antibodies was performed with Fixation/Permeabilization Solution Kit (BD). Secondary antibodies (II Abs) were used to set positive staining gates. Flow cytometry analysis was performed with a FACSCanto II (BD), and data were analyzed using FlowJo software (BD).

Quantitative RT-PCR

Total RNA was prepared with TRIzol (Invitrogen). cDNAs were synthesized with oligo(dT) using Superscript II reverse transcriptase (Invitrogen). qPCR was performed with the ABI 7500 fast real-time PCR system (Applied Biosystems) and SYBR Premix Ex Taq master mix (Takara). Primers are listed in the Key resources table.

In vivo transfer of splenocytes into Rag2^{-/-} recipients

3.10⁶ splenocytes purified from the spleen of WT and mTEC^{ΔMHCII} mice of 8 weeks of age were intravenously injected into Rag2^{-/-} female recipients. CD3⁺, CD4⁺, and CD8⁺ T-cell infiltrates were analyzed 6 weeks after transfer by histology and flow cytometry in different peripheral tissues.

Histology

Tissues were fixed in 10% buffered formalin (Sigma) and embedded in paraffin blocks. 4-µm-thick sections were stained with hematoxylin-eosin (Thermo Fisher) and analyzed by light microscopy (Nikon Statif eclipse Ci-L). For immunofluorescence experiments, frozen thymic sections were stained as previously described (Sergé et al., 2015) with Alexa Fluor 488 or Alexa Fluor 647-conjugated anti-Aire (5H12; eBioscience), biotinylated anti-TPA (LTL; Vector Laboratories), rabbit anti-Fezf2 (F441; IBL Tecan), and rabbit anti-involucrin (BioLegend) antibodies. Rabbit anti-Fezf2 and rabbit anti-involucrin

were revealed with Cy3-conjugated anti-rabbit IgG (Invitrogen), and biotinylated anti-TPA was revealed with Alexa Fluor 488-conjugated streptavidin (Invitrogen). Sections were mounted with Mowiol (Calbiochem). Immunofluorescence confocal microscopy was performed with a LSM780 Leica SP5X confocal microscope. Images were analyzed with ImageJ software.

RNA-seq experiments

Total RNA purified from mTEC^{lo} (**Figure 1—figure supplement 1**) was extracted with miRNeasy Micro Kit (QIAGEN), and RNA quality was assessed on an Agilent 2100 BioAnalyzer (Agilent Technologies). RNA Integrity Number values over 8 were obtained. RNA-seq libraries were generated using the SMART-Seq-v4-Ultra Low Input RNA Kit (Clontech) combined to the Nextera library preparation kit (Illumina) following the manufacturer's instructions. Libraries were sequenced with the Illumina NextSeq 500 machine to generate datasets of single-end 75 bp reads. Two independent biological replicates were used per each condition. RNA-seq data have been deposited with Gene Expression Omnibus (GEO) under the accession number GSE144650.

RNA-seq analysis

The sequencing reads were mapped to the *Mus musculus* (mm10) reference genome using the TopHat 2 (version 2.0.12) aligner (**Kim et al., 2013**). The reads mapping to the annotated genes (igenome UCSC mm10 GTF: https://support.illumina.com/sequencing/sequencing_software/igenome.html) were counted, normalized, and compared using Cuffdiff2 (version 2.2.1; **Trapnell et al., 2013**) between two conditions. Cuffdiff2 generated expression levels as FPKM, FCs, and p-values to assess the statistical significance of the FPKM difference of each gene between the tested two conditions. Genes showing a significant variation in gene expression between WT and Δ CD4, or WT and mTEC ^{Δ MHCII}, or RIPmOVaxOTII-Rag2^{-/-} and OTII-Rag2^{-/-} mice (p-value \leq 0.05, FC difference \geq 2 or \leq 0.5) were considered as up- or downregulated. The TRA and non-TRA gene assignments were obtained from **Sansom et al., 2014**. In this report, the identification of the specificity of expression for each gene in the genome was carried out by analyzing the microarray expression profiles of a large number of different mouse tissues. Aire-dependent, Fezf2-dependent, Aire/Fezf2-dependent, and Aire/Fezf2-independent TRAs were identified using Aire^{-/-} mTEC^{hi} RNA-seq datasets and Fezf2^{-/-} total mTEC microarray datasets, obtained from the NCBI GEO database (GSE87133 and GSE69105, respectively).

Correlation between the variation of gene expression in mTEC^{lo} from WT versus mTEC ^{Δ MHCII} or RIPmOVaxOTII-Rag2^{-/-} versus OTII-Rag2^{-/-} mice, and of the same genes in mTEC^{hi} from WT versus Aire^{-/-} mice was performed doing a locally regression (loess) with the R software (<http://www.r-project.org/>). Differential gene expression in WT versus Aire^{-/-} mTEC^{hi} was obtained by processing using TopHat2 and Cuffdiff2, the sequencing reads corresponding to WT (**Chuprin et al., 2015**) and Aire^{-/-} (**Danan-Gotthold et al., 2016**) mTEC^{hi} RNA-seq datasets, which were obtained from the NCBI GEO database (GSE68190 and GSE87133, respectively). HDAC3-dependent mTEC-specific transcription factors regulated by mTEC-thymocyte crosstalk were identified by comparing the top 50 transcriptional regulators that are induced by HDAC3 (**Goldfarb et al., 2016**) with genes upregulated in the different mouse models. TRAs differentially expressed between mTEC^{lo} from WT and mTEC ^{Δ MHCII} mice were classified according to their tissue distribution using the mouse ENCODE transcriptome database (**Yue, 2014**). Only tissues that showed the highest expression were taken into account.

Single-cell RNA-seq analysis

Single-cell RNA-seq count matrix from **Wells et al., 2020** (accession number GSE137699) was reanalyzed with the Seurat package (**Hao et al., 2021**). QC analysis was performed by filtering out cells with a number of feature counts under 200 or over 4000, and a proportion of mitochondrial counts over 4%. Sample integration was performed as described in the Seurat vignette. After PCA for dimension reduction, 15 first dimensions were conserved. Cells were clustered and visualized with UMAP. Cluster annotation was performed by identifying sets of specific markers to each cluster using a differential expression test (FindMarkers function, test = 'roc'). Heatmaps were generated using the pheatmap R package.

Nano-ChIP-seq experiments

Nano-ChIP-seq was performed as previously described ([Adli and Bernstein, 2011](#)) on $5 \cdot 10^4$ purified mTEC^{lo} ([Figure 1—figure supplement 1](#)). ChIP-seq libraries were prepared with TruSeq ChIP Sample Preparation Kit (Illumina), and 2×75 bp paired-end reads were sequenced on an Illumina HiSeq. ChIP-seq data have been deposited with GEO under the accession number GSE144680.

ChIP-seq analysis

Reads were aligned on the mouse genome (mm10) using Bowtie 2 and default parameters ([Langmead and Salzberg, 2012](#)). Properly paired alignments were selected using Samtools view with the `Ox2flag` (`-f` option). Nonuniquely mapped reads-pairs were filtered out by removing reads with the 'XS' tag set by Bowtie 2. Normalized bedgraphs for ChIP and input samples were generated using MACS2 ([Zhang et al., 2008](#)) with the `callpeak` command in BAMPE mode with the `--SPMR` option. For the diffused H3K27me3 histone mark, the `-broad` option was used. ChIP enrichment was calculated parsing the ChIP and input normalized bedgraphs with MACS2 and the `bdgcmp` command (`-m FE` option). The obtained bedgraphs were converted to wig using the `bedGraphToWig.pl` script with the `--step 10` parameter. MACS2-generated peak calling files were converted to BED files using the `cut -f 1-6` command. The obtained Wig and BED files were parsed by CEAS ([Shin et al., 2009](#)) to generate metagene profile plots corresponding to the average enrichment of H3K4me3 in 3 kb TSS windows or H3K27me3 at gene loci. H3K4me3 and H3K27me3 CEAS-dumped files were parsed to compute ratios of ChIP/input in 1 kb TSS windows and gene loci, respectively. Statistical significance between ChIP enrichment data was tested using the nonparametric Mann–Whitney test. Data were visualized using the Integrative Genomics Viewer (IGV) ([Robinson et al., 2011](#)).

Statistics

Data are presented as means \pm standard error of mean (SEM). Statistical analysis was performed with GraphPad Prism 7.03 software by using ANOVA, chi-square, unpaired Student's *t*-test, or Mann–Whitney test. **** $p < 0.0001$, *** $p < 0.001$, ** $p < 0.01$, * $p < 0.05$. Normal distribution of the data was assessed using d'Agostino–Pearson omnibus normality test.

Acknowledgements

We thank Pr. Arnaud Sergé (LAI, Marseille, France) for critical reading of the manuscript, Pr. Walter Reith (University of Geneva, Switzerland) for providing *Ciita*^{III+IV/-} and *K14xCiita*^{III -/-} mice, and Dr. Bruno Lucas (Institut Cochin, Paris, France) for providing MHCII^{-/-} mice. We also thank Cloé Zamit and Alexia Borelli (CIML, Marseille, France) for help with mouse genotyping and Lionel Chasson (CIML, Marseille, France) for help with paraffin-embedded tissues. We acknowledge the flow cytometry, the imaging core (ImagImm) and animal facility platforms at CIML for excellent technical support. NL and JC were supported by a PhD fellowship from Aix-Marseille University and the Ministère de l'Enseignement Supérieur et de la Recherche, respectively.

Additional information

Funding

Funder	Grant reference number	Author
H2020 Marie Skłodowska-Curie Actions	CIG_SIGnEPI4ToI_618541	Magali Irla
Agence Nationale de la Recherche	2011-CHEX-001-R12004KK	Matthieu Giraud
Agence Nationale de la Recherche	ANR-19-CE18-0021-01 RANKLthym	Magali Irla

The funders had no role in study design, data collection and interpretation, or the decision to submit the work for publication.

Author contributions

Noella Lopes, Formal analysis, Investigation, Methodology, Validation, Writing – original draft; Nicolas Boucherit, Methodology, Validation; Jérémy C Santamaria, Data curation, Formal analysis, Validation; Nathan Provin, Conceptualization, Data curation, Formal analysis, Visualization; Jonathan Charaix, Matthieu Giraud, Data curation, Formal analysis, Methodology, Software, Validation, Writing - review and editing; Pierre Ferrier, Conceptualization, Funding acquisition, Methodology, Supervision, Writing – original draft, Writing - review and editing; Magali Irla, Conceptualization, Data curation, Formal analysis, Funding acquisition, Methodology, Supervision, Visualization, Writing – original draft, Writing - review and editing

Author ORCIDs

Noella Lopes  <http://orcid.org/0000-0002-6296-8426>

Jérémy C Santamaria  <http://orcid.org/0000-0001-7613-3668>

Matthieu Giraud  <http://orcid.org/0000-0002-1208-9677>

Magali Irla  <http://orcid.org/0000-0001-8803-9708>

Ethics

All mice were housed, bred and manipulated under specific pathogen-free conditions at the animal facilities of the CIML (Marseille, France). All experiments were done in accordance with national and European laws for laboratory animal welfare (EEC Council Directive 2010/63/UE), and were approved by the Marseille Ethical Committee for Animal Experimentation (Comité National de Réflexion Ethique sur l'Expérimentation Animale no. 14; Permit Number: 02373.03).

Decision letter and Author response

Decision letter <https://doi.org/10.7554/eLife.69982.sa1>

Author response <https://doi.org/10.7554/eLife.69982.sa2>

Additional files**Supplementary files**

- Supplementary file 1. List of tissue-restricted self-antigens (TRAs) differentially expressed in mTEC^{lo} from WT and Δ CD4 mice.
- Supplementary file 2. List of tissue-restricted self-antigens (TRAs) differentially expressed in mTEC^{lo} from WT and mTEC ^{Δ MHCII} mice.
- Supplementary file 3. List of tissue-restricted self-antigens (TRAs) differentially expressed in mTEC^{lo} from OTII-Rag2^{-/-} and RipmOVAxOTII-Rag2^{-/-} mice.
- Supplementary file 4. Main target organs and fold change associated with the expression of tissue-restricted self-antigens (TRAs) differentially expressed in mTEC^{lo} from WT and mTEC ^{Δ MHCII} mice.
- Transparent reporting form

Data availability

RNA-seq data have been deposited in GEO under the accession number GSE144650. ChIP-seq data have been deposited in GEO under the accession number GSE144680.

The following datasets were generated:

Author(s)	Year	Dataset title	Dataset URL	Database and Identifier
Irla M, Giraud M	2020	mTEC ^{lo} /int RNAseq profiling in three mouse models of impaired mTEC/Tcell crosstalk	https://www.ncbi.nlm.nih.gov/geo/query/acc.cgi?acc=GSE144650	NCBI Gene Expression Omnibus, GSE144650

The following previously published datasets were used:

Author(s)	Year	Dataset title	Dataset URL	Database and Identifier
Wells KL	2020	ingle cell sequencing defines a branched progenitor population of stable medullary thymic epithelial cells	https://www.ncbi.nlm.nih.gov/geo/query/acc.cgi?acc=GSE137699	NCBI Gene Expression Omnibus, GSE137699
Abramson J, Giraud M	2016	Aire-KO MEChI RNAseq profiling	https://www.ncbi.nlm.nih.gov/geo/query/acc.cgi?acc=GSE87133	NCBI Gene Expression Omnibus, GSE87133
Abramson J, Giraud M	2015	Sirt1 is essential for Aire-mediated induction of central immunological tolerance	https://www.ncbi.nlm.nih.gov/geo/query/acc.cgi?acc=GSE68190	NCBI Gene Expression Omnibus, GSE68190

References

- Adli M**, Bernstein BE. 2011. Whole-genome chromatin profiling from limited numbers of cells using nano-ChIP-seq. *Nature Protocols* **6**:1656–1668. DOI: <https://doi.org/10.1038/nprot.2011.402>, PMID: 21959244
- Akiyama T**, Shimo Y, Yanai H, Qin J, Ohshima D, Maruyama Y, Asaumi Y, Kitazawa J, Takayanagi H, Penninger JM, Matsumoto M, Nitta T, Takahama Y, Inoue J-I. 2008. The tumor necrosis factor family receptors RANK and CD40 cooperatively establish the thymic medullary microenvironment and self-tolerance. *Immunity* **29**:423–437. DOI: <https://doi.org/10.1016/j.immuni.2008.06.015>, PMID: 18799149
- Akiyama N**, Shinzawa M, Miyachi M, Yanai H, Tateishi R, Shimo Y, Ohshima D, Matsuo K, Sasaki I, Hoshino K, Wu G, Yagi S, Inoue J, Kaisho T, Akiyama T. 2014. Limitation of immune tolerance-inducing thymic epithelial cell development by Spi-B-mediated negative feedback regulation. *The Journal of Experimental Medicine* **211**:2425–2438. DOI: <https://doi.org/10.1084/jem.20141207>, PMID: 25385757
- Anderson MS**, Venanzi ES, Klein L, Chen Z, Berzins SP, Turley SJ, von Boehmer H, Bronson R, Dierich A, Benoist C, Mathis D. 2002. Projection of an immunological self shadow within the thymus by the aire protein. *Science* **298**:1395–1401. DOI: <https://doi.org/10.1126/science.1075958>, PMID: 12376594
- Asano T**, Okamoto K, Nakai Y, Tsutsumi M, Muro R, Suematsu A, Hashimoto K, Okamura T, Ehata S, Nitta T, Takayanagi H. 2019. Soluble RANKL is physiologically dispensable but accelerates tumour metastasis to bone. *Nature Metabolism* **1**:868–875. DOI: <https://doi.org/10.1038/s42255-019-0104-1>, PMID: 32694743
- Baba T**, Nakamoto Y, Mukaida N. 2009. Crucial contribution of thymic Sirp alpha+ conventional dendritic cells to central tolerance against blood-borne antigens in a CCR2-dependent manner. *Journal of Immunology* **183**:3053–3063. DOI: <https://doi.org/10.4049/jimmunol.0900438>, PMID: 19675159
- Baran-Gale J**, Morgan MD, Maio S, Dhalla F, Calvo-Asensio I, Deadman ME, Handel AE, Maynard A, Chen S, Green F, Sit RV, Neff NF, Darmanis S, Tan W, May AP, Marioni JC, Ponting CP, Holländer GA. 2020. Ageing compromises mouse thymus function and remodels epithelial cell differentiation. *eLife* **9**:e56221. DOI: <https://doi.org/10.7554/eLife.56221>, PMID: 32840480
- Barnden MJ**, Allison J, Heath WR, Carbone FR. 1998. Defective TCR expression in transgenic mice constructed using cDNA-based alpha- and beta-chain genes under the control of heterologous regulatory elements. *Immunology and Cell Biology* **76**:34–40. DOI: <https://doi.org/10.1046/j.1440-1711.1998.00709.x>, PMID: 9553774
- Borelli A**, Irla M. 2021. Lymphotoxin: from the physiology to the regeneration of the thymic function. *Cell Death and Differentiation* **28**:2305–2314. DOI: <https://doi.org/10.1038/s41418-021-00834-8>, PMID: 34290396
- Bornstein C**, Nevo S, Giladi A, Kadouri N, Pouzolles M, Gerbe F, David E, Machado A, Chuprin A, Tóth B, Goldberg O, Itzkovitz S, Taylor N, Jay P, Zimmermann VS, Abramson J, Amit I. 2018. Single-cell mapping of the thymic stroma identifies IL-25-producing tuft epithelial cells. *Nature* **559**:622–626. DOI: <https://doi.org/10.1038/s41586-018-0346-1>, PMID: 30022162
- Burkly L**, Hession C, Ogata L, Reilly C, Marconi LA, Olson D, Tizard R, Cate R, Lo D. 1995. Expression of relB is required for the development of thymic medulla and dendritic cells. *Nature* **373**:531–536. DOI: <https://doi.org/10.1038/373531a0>, PMID: 7845467
- Cédile O**, Løbner M, Toft-Hansen H, Frank I, Włodarczyk A, Irla M, Owens T. 2014. Thymic CCL2 influences induction of T-cell tolerance. *Journal of Autoimmunity* **55**:73–85. DOI: <https://doi.org/10.1016/j.jaut.2014.07.004>, PMID: 25129504
- Chuprin A**, Avin A, Goldfarb Y, Herzig Y, Levi B, Jacob A, Sela A, Katz S, Grossman M, Guyon C, Rathaus M, Cohen HY, Sagi I, Giraud M, McBurney MW, Husebye ES, Abramson J. 2015. The deacetylase Sirt1 is an essential regulator of Aire-mediated induction of central immunological tolerance. *Nature Immunology* **16**:737–745. DOI: <https://doi.org/10.1038/ni.3194>, PMID: 26006015

- Cowan JE, Baik S, McCarthy NI, Parnell SM, White AJ, Jenkinson WE, Anderson G. 2018. Aire controls the recirculation of murine Foxp3⁺ regulatory T-cells back to the thymus. *European Journal of Immunology* **48**:844–854. DOI: <https://doi.org/10.1002/eji.201747375>, PMID: 29285761
- Danan-Gotthold M, Guyon C, Giraud M, Levanon EY, Abramson J. 2016. Extensive RNA editing and splicing increase immune self-representation diversity in medullary thymic epithelial cells. *Genome Biology* **17**:219. DOI: <https://doi.org/10.1186/s13059-016-1079-9>
- Derbinski J., Schulte A, Kyewski B, Klein L. 2001. Promiscuous gene expression in medullary thymic epithelial cells mirrors the peripheral self. *Nature Immunology* **2**:1032–1039. DOI: <https://doi.org/10.1038/ni723>, PMID: 11600886
- Derbinski Jens, Gäbler J, Brors B, Tierling S, Jonnakuty S, Hergenahm M, Peltonen L, Walter J, Kyewski B. 2005. Promiscuous gene expression in thymic epithelial cells is regulated at multiple levels. *The Journal of Experimental Medicine* **202**:33–45. DOI: <https://doi.org/10.1084/jem.20050471>, PMID: 15983066
- Dhalla F, Baran-Gale J, Maio S, Chappell L, Holländer GA, Ponting CP. 2020. Biologically indeterminate yet ordered promiscuous gene expression in single medullary thymic epithelial cells. *The EMBO Journal* **39**:e101828. DOI: <https://doi.org/10.15252/emj.2019101828>, PMID: 31657037
- Gäbler J, Arnold J, Kyewski B. 2007. Promiscuous gene expression and the developmental dynamics of medullary thymic epithelial cells. *European Journal of Immunology* **37**:3363–3372. DOI: <https://doi.org/10.1002/eji.200737131>, PMID: 18000951
- Giraud M, Yoshida H, Abramson J, Rahl PB, Young RA, Mathis D, Benoist C. 2012. Aire unleashes stalled RNA polymerase to induce ectopic gene expression in thymic epithelial cells. *PNAS* **109**:535–540. DOI: <https://doi.org/10.1073/pnas.1119351109>, PMID: 22203960
- Goldfarb Y, Kadouri N, Levi B, Sela A, Herzig Y, Cohen RN, Hollenberg AN, Abramson J. 2016. HDAC3 Is a Master Regulator of mTEC Development. *Cell Reports* **15**:651–665. DOI: <https://doi.org/10.1016/j.celrep.2016.03.048>, PMID: 27068467
- Gray DHD, Seach N, Ueno T, Milton MK, Liston A, Lew AM, Goodnow CC, Boyd RL. 2006. Developmental kinetics, turnover, and stimulatory capacity of thymic epithelial cells. *Blood* **108**:3777–3785. DOI: <https://doi.org/10.1182/blood-2006-02-004531>, PMID: 16896157
- Gray D, Abramson J, Benoist C, Mathis D. 2007. Proliferative arrest and rapid turnover of thymic epithelial cells expressing Aire. *The Journal of Experimental Medicine* **204**:2521–2528. DOI: <https://doi.org/10.1084/jem.20070795>, PMID: 17908938
- Haljasorg U, Dooley J, Laan M, Kisand K, Bichele R, Liston A, Peterson P. 2017. Irf4 Expression in Thymic Epithelium Is Critical for Thymic Regulatory T Cell Homeostasis. *Journal of Immunology* **198**:1952–1960. DOI: <https://doi.org/10.4049/jimmunol.1601698>, PMID: 28108558
- Handel AE, Shikama-Dorn N, Zhanybekova S, Maio S, Graedel AN, Zuklys S, Ponting CP, Holländer GA. 2018. Comprehensively Profiling the Chromatin Architecture of Tissue Restricted Antigen Expression in Thymic Epithelial Cells Over Development. *Frontiers in Immunology* **9**:2120. DOI: <https://doi.org/10.3389/fimmu.2018.02120>, PMID: 30283453
- Hao Y, Hao S, Andersen-Nissen E, Mauck WM, Zheng S, Butler A, Lee MJ, Wilk AJ, Darby C, Zager M, Hoffman P, Stoeckius M, Papalexi E, Mimitou EP, Jain J, Srivastava A, Stuart T, Fleming LM, Yeung B, Rogers AJ, et al. 2021. Integrated analysis of multimodal single-cell data. *Cell* **184**:3573–3587. DOI: <https://doi.org/10.1016/j.cell.2021.04.048>, PMID: 34062119
- Hikosaka Y, Nitta T, Ohigashi I, Yano K, Ishimaru N, Hayashi Y, Matsumoto M, Matsuo K, Penninger JM, Takayanagi H, Yokota Y, Yamada H, Yoshikai Y, Inoue J-I, Akiyama T, Takahama Y. 2008. The cytokine RANKL produced by positively selected thymocytes fosters medullary thymic epithelial cells that express autoimmune regulator. *Immunity* **29**:438–450. DOI: <https://doi.org/10.1016/j.immuni.2008.06.018>, PMID: 18799150
- Hu Z, Lancaster JN, Sasiponganan C, Ehrlich LIR. 2015. CCR4 promotes medullary entry and thymocyte-dendritic cell interactions required for central tolerance. *The Journal of Experimental Medicine* **212**:1947–1965. DOI: <https://doi.org/10.1084/jem.20150178>, PMID: 26417005
- Irla M, Hugues S, Gill J, Nitta T, Hikosaka Y, Williams IR, Hubert FX, Scott HS, Takahama Y, Holländer GA, Reith W. 2008. Autoantigen-specific interactions with CD4⁺ thymocytes control mature medullary thymic epithelial cell cellularity. *Immunity* **29**:451–463. DOI: <https://doi.org/10.1016/j.immuni.2008.08.007>, PMID: 18799151
- Irla M, Hollander G, Reith W. 2010. Control of central self-tolerance induction by autoreactive CD4⁺ thymocytes. *Trends in Immunology* **31**:71–79. DOI: <https://doi.org/10.1016/j.it.2009.11.002>, PMID: 20004147
- Irla M, Guerri L, Guenot J, Sergé A, Lantz O, Liston A, Imhof BA, Palmer E, Reith W. 2012. Antigen recognition by autoreactive CD4⁺ thymocytes drives homeostasis of the thymic medulla. *PLOS ONE* **7**:e52591. DOI: <https://doi.org/10.1371/journal.pone.0052591>, PMID: 23300712
- Irla M. 2020. RANK Signaling in the Differentiation and Regeneration of Thymic Epithelial Cells. *Frontiers in Immunology* **11**:623265. DOI: <https://doi.org/10.3389/fimmu.2020.623265>
- Kadouri N, Nevo S, Goldfarb Y, Abramson J. 2020. Thymic epithelial cell heterogeneity: TEC by TEC. *Nature Reviews. Immunology* **20**:239–253. DOI: <https://doi.org/10.1038/s41577-019-0238-0>, PMID: 31804611
- Kim D, Perrea G, Trapnell C, Pimentel H, Kelley R, Salzberg SL. 2013. TopHat2: accurate alignment of transcriptomes in the presence of insertions, deletions and gene fusions. *Genome Biology* **14**:R36. DOI: <https://doi.org/10.1186/gb-2013-14-4-r36>, PMID: 23618408
- Klein L, Kyewski B, Allen PM, Hogquist KA. 2014. Positive and negative selection of the T cell repertoire: what thymocytes see (and don't see). *Nature Reviews. Immunology* **14**:377–391. DOI: <https://doi.org/10.1038/nri3667>, PMID: 24830344

- Klein L, Robey EA, Hsieh CS. 2019. Central CD4⁺ T cell tolerance: deletion versus regulatory T cell differentiation. *Nature Reviews. Immunology* **19**:7–18. DOI: <https://doi.org/10.1038/s41577-018-0083-6>, PMID: 30420705
- Koh AS, Miller EL, Buenrostro JD, Moskowitz DM, Wang J, Greenleaf WJ, Chang HY, Crabtree GR. 2018. Rapid chromatin repression by Aire provides precise control of immune tolerance. *Nature Immunology* **19**:162–172. DOI: <https://doi.org/10.1038/s41590-017-0032-8>, PMID: 29335648
- Kolde R. 2018. pheatmap. b333453. GitHub. <https://github.com/raivokolde/pheatmap>
- Kurts C, Heath WR, Carbone FR, Allison J, Miller JF, Kosaka H. 1996. Constitutive class I-restricted exogenous presentation of self antigens in vivo. *The Journal of Experimental Medicine* **184**:923–930. DOI: <https://doi.org/10.1084/jem.184.3.923>, PMID: 9064352
- Kyewski B, Klein L. 2006. A central role for central tolerance. *Annual Review of Immunology* **24**:571–606. DOI: <https://doi.org/10.1146/annurev.immunol.23.021704.115601>, PMID: 16551260
- Langmead B, Salzberg SL. 2012. Fast gapped-read alignment with Bowtie 2. *Nature Methods* **9**:357–359. DOI: <https://doi.org/10.1038/nmeth.1923>, PMID: 22388286
- LeibundGut-Landmann S, Waldburger J-M, Reis e Sousa C, Acha-Orbea H, Reith W. 2004. MHC class II expression is differentially regulated in plasmacytoid and conventional dendritic cells. *Nature Immunology* **5**:899–908. DOI: <https://doi.org/10.1038/ni1109>, PMID: 15322541
- Lkhagvasuren E, Sakata M, Ohigashi I, Takahama Y. 2013. Lymphotoxin β receptor regulates the development of CCL21-expressing subset of postnatal medullary thymic epithelial cells. *Journal of Immunology* **190**:5110–5117. DOI: <https://doi.org/10.4049/jimmunol.1203203>, PMID: 23585674
- Lomada D, Liu B, Coghlan L, Hu Y, Richie ER. 2007. Thymus medulla formation and central tolerance are restored in IKK α −/− mice that express an IKK α transgene in keratin 5+ thymic epithelial cells. *Journal of Immunology* **178**:829–837. DOI: <https://doi.org/10.4049/jimmunol.178.2.829>, PMID: 17202344
- Lopes N, Serge A, Ferrier P, Irla M. 2015. Thymic Crosstalk Coordinates Medulla Organization and T-Cell Tolerance Induction. *Frontiers in Immunology* **6**:365. DOI: <https://doi.org/10.3389/fimmu.2015.00365>
- Lopes N, Vachon H, Marie J, Irla M. 2017. Administration of RANKL boosts thymic regeneration upon bone marrow transplantation. *EMBO Molecular Medicine* **9**:835–851. DOI: <https://doi.org/10.15252/emmm.201607176>, PMID: 28455312
- Lopes N, Charaix J, Cedile O, Serge A, Irla M. 2018. Lymphotoxin α fine-tunes T cell clonal deletion by regulating thymic entry of antigen-presenting cells. *Nature Communications* **9**:1262. DOI: <https://doi.org/10.1038/s41467-018-03619-9>
- Madsen L, Labrecque N, Engberg J, Dierich A, Svejgaard A, Benoist C, Mathis D, Fugger L. 1999. Mice lacking all conventional MHC class II genes. *PNAS* **96**:10338–10343. DOI: <https://doi.org/10.1073/pnas.96.18.10338>, PMID: 10468609
- Metzger TC, Khan IS, Gardner JM, Mouchess ML, Johannes KP, Krawisz AK, Skrzypczynska KM, Anderson MS. 2013. Lineage tracing and cell ablation identify a post-Aire-expressing thymic epithelial cell population. *Cell Reports* **5**:166–179. DOI: <https://doi.org/10.1016/j.celrep.2013.08.038>, PMID: 24095736
- Michel C, Miller CN, Kuchler R, Brors B, Anderson MS, Kyewski B, Pinto S. 2017. Revisiting the Road Map of Medullary Thymic Epithelial Cell Differentiation. *Journal of Immunology* **199**:3488–3503. DOI: <https://doi.org/10.4049/jimmunol.1700203>, PMID: 28993517
- Miller CN, Proekt I, von Moltke J, Wells KL, Rajpurkar AR, Wang H, Rattay K, Khan IS, Metzger TC, Pollack JL, Fries AC, Lwin WW, Wigton EJ, Parent AV, Kyewski B, Erle DJ, Hogquist KA, Steinmetz LM, Locksley RM, Anderson MS. 2018. Thymic tuft cells promote an IL-4-enriched medulla and shape thymocyte development. *Nature* **559**:627–631. DOI: <https://doi.org/10.1038/s41586-018-0345-2>, PMID: 30022164
- Nishikawa Y, Hirota F, Yano M, Kitajima H, Miyazaki J, Kawamoto H, Mouri Y, Matsumoto M. 2010. Biphasic Aire expression in early embryos and in medullary thymic epithelial cells before end-stage terminal differentiation. *The Journal of Experimental Medicine* **207**:963–971. DOI: <https://doi.org/10.1084/jem.20092144>
- Org T, Rebane A, Kisand K, Laan M, Haljasorg U, Andreson R, Peterson P. 2009. AIRE activated tissue specific genes have histone modifications associated with inactive chromatin. *Human Molecular Genetics* **18**:4699–4710. DOI: <https://doi.org/10.1093/hmg/ddp433>, PMID: 19744957
- Otero DC, Baker DP, David M. 2013. IRF7-Dependent IFN- β Production in Response to RANKL Promotes Medullary Thymic Epithelial Cell Development. *Journal of Immunology* **10**:1203086. DOI: <https://doi.org/10.4049/jimmunol.1203086>
- Pezzi N, Assis AF, Cotrim-Sousa LC, Lopes GS, Mosella MS, Lima DS, Bombonato-Prado KF, Passos GA. 2016. Aire knockdown in medullary thymic epithelial cells affects Aire protein, deregulates cell adhesion genes and decreases thymocyte interaction. *Molecular Immunology* **77**:157–173. DOI: <https://doi.org/10.1016/j.molimm.2016.08.003>, PMID: 27505711
- Riemann M, Andreas N, Fedoseeva M, Meier E, Weih D, Freytag H, Schmidt-Ullrich R, Klein U, Wang ZQ, Weih F. 2017. Central immune tolerance depends on crosstalk between the classical and alternative NF- κ B pathways in medullary thymic epithelial cells. *Journal of Autoimmunity* **81**:56–67. DOI: <https://doi.org/10.1016/j.jaut.2017.03.007>, PMID: 28385374
- Robinson JT, Thorvaldsdóttir H, Winckler W, Guttman M, Lander ES, Getz G, Mesirov JP. 2011. Integrative genomics viewer. *Nature Biotechnology* **29**:24–26. DOI: <https://doi.org/10.1038/nbt.1754>, PMID: 21221095
- Rodrigues PM, Ribeiro AR, Perrod C, Landry JJM, Araújo L, Pereira-Castro I, Benes V, Moreira A, Xavier-Ferreira H, Meireles C, Alves NL. 2017. Thymic epithelial cells require p53 to support their long-term function in thymopoiesis in mice. *Blood* **130**:478–488. DOI: <https://doi.org/10.1182/blood-2016-12-758961>, PMID: 28559356

- Sansom SN**, Shikama-Dorn N, Zhanybekova S, Nusspaumer G, Macaulay IC, Deadman ME, Heger A, Ponting CP, Holländer GA. 2014. Population and single-cell genomics reveal the Aire dependency, relief from Polycomb silencing, and distribution of self-antigen expression in thymic epithelia. *Genome Research* **24**:1918–1931. DOI: <https://doi.org/10.1101/gr.171645.113>, PMID: 25224068
- Sergé A**, Bailly A-L, Aurrand-Lions M, Imhof BA, Irla M. 2015. For3D: Full organ reconstruction in 3D, an automatized tool for deciphering the complexity of lymphoid organs. *Journal of Immunological Methods* **424**:32–42. DOI: <https://doi.org/10.1016/j.jim.2015.04.019>, PMID: 25956038
- Shen H**, Ji Y, Xiong Y, Kim H, Zhong X, Jin MG, Shah YM, Omary MB, Liu Y, Qi L, Rui L. 2019. Medullary thymic epithelial NF- κ B-inducing kinase (NIK)/IKK α pathway shapes autoimmunity and liver and lung homeostasis in mice. *PNAS* **116**:19090–19097. DOI: <https://doi.org/10.1073/pnas.1901056116>, PMID: 31481626
- Shin H**, Liu T, Manrai AK, Liu XS. 2009. CEAS: cis-regulatory element annotation system. *Bioinformatics* **25**:2605–2606. DOI: <https://doi.org/10.1093/bioinformatics/btp479>, PMID: 19689956
- Shinkai Y**, Rathbun G, Lam KP, Oltz EM, Stewart V, Mendelsohn M, Charron J, Datta M, Young F, Stall AM. 1992. RAG-2-deficient mice lack mature lymphocytes owing to inability to initiate V(D)J rearrangement. *Cell* **68**:855–867. DOI: [https://doi.org/10.1016/0092-8674\(92\)90029-c](https://doi.org/10.1016/0092-8674(92)90029-c), PMID: 1547487
- Takaba H**, Morishita Y, Tomofuji Y, Danks L, Nitta T, Komatsu N, Kodama T, Takayanagi H. 2015. Fezf2 Orchestrates a Thymic Program of Self-Antigen Expression for Immune Tolerance. *Cell* **163**:975–987. DOI: <https://doi.org/10.1016/j.cell.2015.10.013>, PMID: 26544942
- Trapnell C**, Hendrickson DG, Sauvageau M, Goff L, Rinn JL, Pachter L. 2013. Differential analysis of gene regulation at transcript resolution with RNA-seq. *Nature Biotechnology* **31**:46–53. DOI: <https://doi.org/10.1038/nbt.2450>, PMID: 23222703
- Tykocinski LO**, Sinemus A, Rezavandy E, Weiland Y, Baddeley D, Cremer C, Sonntag S, Willecke K, Derbinski J, Kyewski B. 2010. Epigenetic regulation of promiscuous gene expression in thymic medullary epithelial cells. *PNAS* **107**:19426–19431. DOI: <https://doi.org/10.1073/pnas.1009265107>, PMID: 20966351
- Ucar O**, Rattay K. 2015. Promiscuous Gene Expression in the Thymus: A Matter of Epigenetics, miRNA, and More? *Frontiers in Immunology* **6**:93. DOI: <https://doi.org/10.3389/fimmu.2015.00093>, PMID: 25784915
- Ueno T**, Saito F, Gray DHD, Kuse S, Hieshima K, Nakano H, Kakiuchi T, Lipp M, Boyd RL, Takahama Y. 2004. CCR7 signals are essential for cortex-medulla migration of developing thymocytes. *The Journal of Experimental Medicine* **200**:493–505. DOI: <https://doi.org/10.1084/jem.20040643>, PMID: 15302902
- van Ewijk W**, Shores EW, Singer A. 1994. Crosstalk in the mouse thymus. *Immunology Today* **15**:214–217. DOI: [https://doi.org/10.1016/0167-5699\(94\)90246-1](https://doi.org/10.1016/0167-5699(94)90246-1), PMID: 8024681
- Waldburger JM**, Rossi S, Hollander GA, Rodewald HR, Reith W, Acha-Orbea H. 2003. Promoter IV of the class II transactivator gene is essential for positive selection of CD4+ T cells. *Blood* **101**:3550–3559. DOI: <https://doi.org/10.1182/blood-2002-06-1855>, PMID: 12506036
- Wells KL**, Miller CN, Gschwind AR, Wei W, Phipps JD, Anderson MS, Steinmetz LM. 2020. Combined transient ablation and single-cell RNA-sequencing reveals the development of medullary thymic epithelial cells. *eLife* **9**:e60188. DOI: <https://doi.org/10.7554/eLife.60188>, PMID: 33226342
- White AJ**, Jenkinson WE, Cowan JE, Parnell SM, Bacon A, Jones ND, Jenkinson EJ, Anderson G. 2014. An essential role for medullary thymic epithelial cells during the intrathymic development of invariant NKT cells. *Journal of Immunology* **192**:2659–2666. DOI: <https://doi.org/10.4049/jimmunol.1303057>, PMID: 24510964
- Wong K**, Lister NL, Barsanti M, Lim JMC, Hammett MV, Khong DM, Siatskas C, Gray DHD, Boyd RL, Chidgey AP. 2014. Multilineage potential and self-renewal define an epithelial progenitor cell population in the adult thymus. *Cell Reports* **8**:1198–1209. DOI: <https://doi.org/10.1016/j.celrep.2014.07.029>, PMID: 25131206
- Youm YH**, Horvath TL, Mangelsdorf DJ, Kliewer SA, Dixit VD. 2016. Prolongevity hormone FGF21 protects against immune senescence by delaying age-related thymic involution. *PNAS* **113**:1026–1031. DOI: <https://doi.org/10.1073/pnas.1514511113>, PMID: 26755598
- Yue F**. 2014. A comparative encyclopedia of DNA elements in the mouse genome. *Nature* **515**:355–364. DOI: <https://doi.org/10.1038/nature13992>
- Zhang B**, Wang Z, Ding J, Peterson P, Gunning WT, Ding HF. 2006. NF- κ B2 is required for the control of autoimmunity by regulating the development of medullary thymic epithelial cells. *The Journal of Biological Chemistry* **281**:38617–38624. DOI: <https://doi.org/10.1074/jbc.M606705200>, PMID: 17046818
- Zhang Y**, Liu T, Meyer CA, Eeckhoute J, Johnson DS, Bernstein BE, Nusbaum C, Myers RM, Brown M, Li W, Liu XS. 2008. Model-based analysis of ChIP-Seq (MACS). *Genome Biology* **9**:R137. DOI: <https://doi.org/10.1186/gb-2008-9-9-r137>, PMID: 18798982
- Zhu M**, Chin RK, Christiansen PA, Lo JC, Liu X, Ware C, Siebenlist U, Fu YX. 2006. NF- κ B2 is required for the establishment of central tolerance through an Aire-dependent pathway. *The Journal of Clinical Investigation* **116**:2964–2971. DOI: <https://doi.org/10.1172/JCI28326>, PMID: 17039258
- Žuklys S**, Handel A, Zhanybekova S, Govani F, Keller M, Maio S, Mayer CE, Teh HY, Hafen K, Gallone G, Barthlott T, Ponting CP, Holländer GA. 2016. Foxn1 regulates key target genes essential for T cell development in postnatal thymic epithelial cells. *Nature Immunology* **17**:1206–1215. DOI: <https://doi.org/10.1038/ni.3537>, PMID: 27548434